Politecnico di Milano
Scuola di Ingegneria Industriale e dell'Informazione
Corso di Laurea Magistrale in Electrical Engineering

Distributed Secondary Frequency Control in Multibus Islanded Microgrids

Relatore: Prof. Alberto Berizzi
Correlatore: Dott. Pietro Raboni

Tesi di laurea di:
Guido Recalcati Matr. 875014

Anno Accademico 2017–2018

To Monica

Abstract

This thesis was developed in collaboration with Engie-EPS and deals with the secondary frequency control of the isolated microgrid of Anjouan, an island of the Comores archipelago. Isolated Microgrids present many different control challenges, mainly deriving from their low short-circuit capacity, high penetration of renewable energy sources, and low inertia, due to the high presence of power electronic-based generators. Frequency control, therefore, is crucial, as the grid is highly sensitive to perturbations and changes. In addition, the grid of Anjouan also features a multi-bus structure, which implies the use of long communication system based on the local infrastructure (built and owned by a third party), which is not considered reliable enough. In this context, we could not exploit a traditional centralized frequency control structure, which is too sensitive to communication failures. The aim of the thesis, therefore, is to realize a secondary frequency controller which is more robust against loss of communication. To do this, we exploited a distributed structure, which does not rely solely on the links between a central unit and distributed generators, but makes also use of information exchange between neighboring generators. We operated an analytical study of the controller using Lyapunov theory and graph theory, and we tested its performances using Matlab Simulink and DIgSILENT PowerFactory. The simulation results show how the controller is able to operate primary and secondary frequency regulations even with multiple communication faults.

Sommario

Questa tesi è stata sviluppata in collaborazione con Engie-EPS, e tratta della regolazione secondaria di frequenza nella microgrid isolata dell'isola di Anjouan, nell'arcipelago delle Comore. Le microgrid isolate presentano diversi problemi dal punto di vista del controllo, principalmente derivanti dalla loro bassa potenza di corto circuito, dall'alta penetrazione di fonti energetiche rinnovabili e dalla bassa inerzia causata dalla grande presenza di inverter. Il controllo di frequenza è quindi di significativa importanza, poichè la rete è molto sensibile alle perturbazioni. Oltre a questi aspetti, la rete di Anjouan è anche caratterizzata da una topologia multisbarra, che rende necessario l'utilizzo di un complesso sistema di comunicazioni, basato sull'infrastruttura locale (costruita ed esercita da un'azienda terza), considerata non sufficientemente affidabile. In questo contesto, non si è ritenuto possibile utilizzare una tradizionale struttura di controllo centralizzato, in quanto troppo sensibile ai guasti nelle comunicazioni. Lo scopo di questa tesi è quindi quello di realizzare un regolatore secondario di frequenza più robusto rispetto alle perdite di comunicazione. Per fare ciò, si è scelto di sfruttare un'architettura distribuita, che non fa affidamento unicamente sui collegamenti tra unità centrale e generatori distribuiti, ma sfrutta anche le informazioni scambiate tra generatori vicini. Si è svolto uno studio analitico del controllore proposto, utilizzando la teoria di Lyapunov e la teoria dei grafi e si sono valutate le performance del sistema utilizzando Matlab Simulink e DIgSILENT PowerFactory. I risultati delle simulazioni mostrano come il sistema di controllo proposto sia in grado di attuare le regolazioni primaria e secondaria anche in caso di diversi guasti alle comunicazioni.

Contents

List of Figures

List of Tables

Introduction

With the rise of distributed generation systems, the grid is constantly facing new challenges. New means of energy production, such as small photovoltaic plants and other renewable energy sources, cause power flow to be bidirectional rather than unidirectional, as it has always traditionally been. This means that energy is not only flowing from large power plants to users, but also vice-versa [1]. Moreover, renewable power is tipically intermittent and this generates control problems, particularly regarding grid forecasting and scheduling [2]. To solve the problems associated with this new situations, the grid must be more and more smart, flexible and adaptive to changes. In this challenging context, Microgrids serve as a way to integrate power production and consumption in a singular entity [3], which can be considered as a single dispatchable load. In literature we can find a few Microgrid definitions, such as:

- From the U.S. Department of Energy Microgrid Exchange Group [4] : *"A microgrid is a group of interconnected loads and distributed energy resources within clearly defined electrical boundaries that acts as a single controllable entity with respect to the grid. A microgrid can connect and disconnect from the grid to enable it to operate in both grid-connected or island-mode"*;
- From European research project [5] : "*Microgrids comprise Low Voltage distribution systems with distributed energy sources, such as micro-turbines, fuel cells, PVs, etc., together with storage devices, i.e. flywheels, energy capacitors and batteries, and controllable loads, offering considerable control capabilities over the network operation. These systems are interconnected to the Medium Voltage Distribution network, but they can be also operated isolated from the main grid, in case of faults in the upstream network*".

In general, we can say that a Microgrid is different from a traditional power system for its smaller size and for the high penetration of res, sometimes coupled with storage. Moreover, when operated in islanded mode, Microgrid present a peculiar set of problems which make the control even more challenging. As a matter of fact, the presence of different types of generation and storage system implies a thorough

penetration of power electronics in Microgrids and therefore they generally present a lower inertia. This, together with the usually low short-circuit capacity, can result in relatively large voltage and frequency deviations after perturbations [6].
The Engie-EPS team is specialized in islanded Microgrids and this thesis was developed within one of such projects. The developed project is focused on the revamping of the grid of Anjouan (Comores), which will be characterized by three power plants spread throughout the island, with particular interest to secondary frequency control. The grid configuration implies a three-bus structure, which requires a communication system to be implemented for control purposes. This communication network is based on the public internet infrastructure through a VPN, and so it could be influenced by high traffic on the lines, causing delays or communication losses between the central controller and the generators. We therefore needed to implement a system robust to this kind of failures.
The objective of the thesis is to design and test a distributed system for the secondary frequency regulation of the island, as a solution to communication uncertainties. We chose a distributed architecture, as opposed to a centralized traditional one, as it does not rely solely on communications between a central unit and the generators but, in our case, it exploits also a secondary communication network between generators.
We operated an analytical study of the controller using Lyapunov and graph theories, and we tested its performances using Simulink and DIgSILENT PowerFactory.
This thesis is divided in 5 chapters which are articulated as follows:

- *Chapter 1 - Microgrid Control Generalities.* In this chapter we introduce the traditional approach to frequency regulation in its primary and secondary levels. In particular, we discuss the issues associated with the centralized secondary regulation.

- *Chapter 2 - Distributed Control.* After recalling some important concepts about graph theory and Lyapunov theory, we propose a secondary frequency controller which exploits a distributed architecture.

- *Chapter 3 - Simulations.* In this chapter, we test the robustness of the controller we designed, using Simulink. In particular, we observe the behavior of the system under different communication scenarios, considering a load perturbation.

- *Chapter 4 - Study case: the grid of Anjouan, Comores.* In this chapter we introduce the features of the grid we realized the controller for, and we report the details of the DIgSILENT PowerFactory model we created.

- *Chapter 5 - Simulations with DIgSILENT PowerFactory.* In this chapter we show the results of the simulation we performed using PowerFactory, testing the controller in a grid environment, with various cases of communication loss.

Chapter 1

Microgrid Control Generality

In this chapter, after a brief introduction to Microgrids, we will discuss the traditional approach to frequency regulation. In large power systems, this task is usually carried out by three different control levels: primary regulation, secondary regulation and tertiary regulation. In the following pages, we will explain the fundamentals of the first two levels (as the third one is of economic interest, and not related to the aim of this thesis), focusing on steady-state behavior and control scheme. We will also introduce the main issue discussed in the thesis, that is the centralized nature of the secondary control.

1.1 The need for control

Any electric power system should work at a constant frequency (usually 50 Hz or 60 Hz) in order to ensure the correct operation of all the connected loads and users [7]. In a traditional power system (supplied with rotating machines), the frequency is related to the rotational speed of the generators, which remains constant only if the prime mover torque is equal to the electromagnetic torque [8]. This relation is represented by equation 1.1:

$$J\dot{\omega}_m = T_m - T_e \tag{1.1}$$

Where J is the total moment of inertia of the rotor masses in $Kg \cdot m^2$, $\dot{\omega}_m$ is the time derivative of the rotational speed of the rotor with respect to a stationary axis, in mechanical radiants per second, and T_m and T_e are the previously mentioned prime mover and electromagnetic torque in $N \cdot m$.
In fact, the balance between the two torques is constantly disturbed by changes in power requested by the loads (connection and disconnection of users, faults...) and variations in power supplied by the generators. The result is a variation in the speed of the rotors and, therefore, a variation in the system frequency. It is important to notice how, by mentioning a "system frequency", we are implicitly

making the assumption of a rigid system, that is, we are assuming that the rotors of the various generators are all moving at the same speed, neglecting electromechanical oscillations . In other words, we are assuming that the period of oscillations is significantly smaller than the duration of the phenomena we are interested in, so that we can consider all of the machines as synchronously moving at the rotor speed correspondent to the system frequency.
The objective of the frequency regulation, therefore, is to keep the system frequency in a band of acceptable values around the reference, while balancing power request and power supply. We will now explain the details of this kind of control.

1.2 First Level (Primary control)

1.2.1 Steady state behavior

This first control layer has the objective of balancing power generation and power request, in order to stabilize the grid after a load variation. The most common strategy implies the use of the well known droop technique [9] . This technique can be implemented in the inverters to emulate the behavior of a synchronous machine, linking active power and frequency through the steady-state characteristic curve shown in Fig 1.1 and described by eq. 1.2.

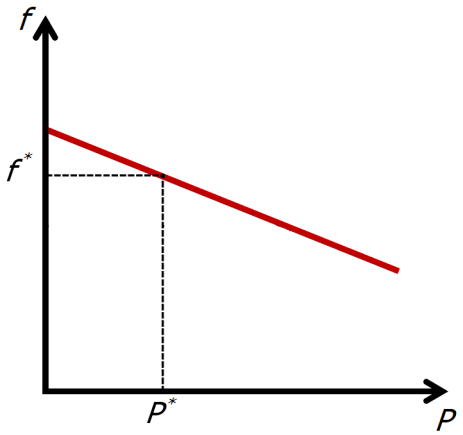

Figure 1.1: Droop curve example

$$f(t) - f^* = m(P(t) - P^*) \tag{1.2}$$

Where f and P are respectively frequency and power output values, f^* and P^* are their reference values and indicate the normal working point, and m is the proportional droop coefficient, typically set between 1% and 8%. It is important to notice how, after the transient due to a load change, the final frequency is different from the reference one. Indeed, if at first the generator is at the operating point A (P_A, f_A)

and the load changes from P_A to a higherP_B, the working point will move along the characteristic, up to a final f_B lower than f_A (see Fig 1.2). Vice versa when the load decreases, the final frequency f_B is higher. The primary regulation, therefore, introduces a steady-state frequency error which has to be corrected by the secondary regulation.

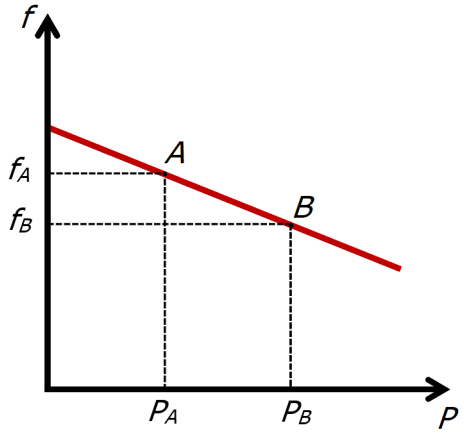

Figure 1.2: Load variation example

1.2.2 Control scheme

If we solve eq. 1.2 for P and then we use Laplace transform, we obtain the block scheme shown in Fig. 1.3. Notice that this is a small signal model, so all the variables will be expressed in variations (Δf^* and ΔP^* are the references for frequency and power variations, Δf is the output frequency variation).

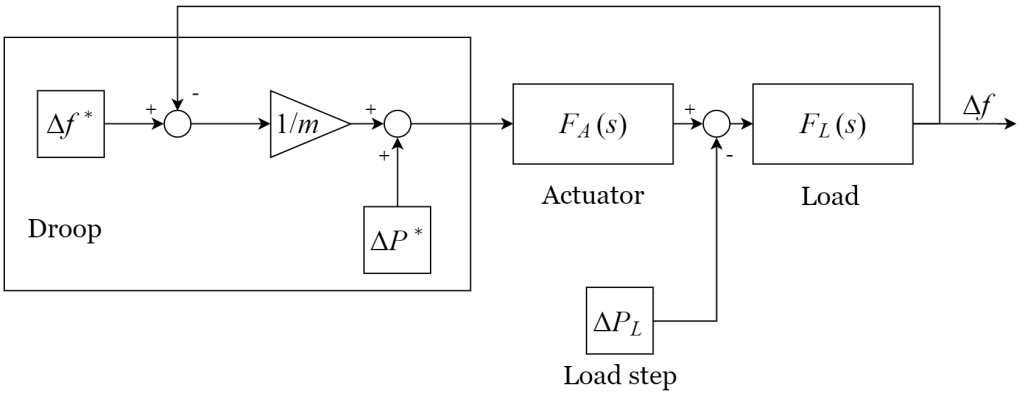

Figure 1.3: Primary regulation scheme

As we can see, the droop method produces an output power that the actuator will receive as the reference [10] [11]. This component, which represents the dynamic behavior of the generator as simplified to first order transfer function, will then

follow the reference and supply the load. It is important to highlight how the two references values $\Delta f^*$and $\Delta P^*$are often set to 0, so in future schemes we will not include them.

1.2.3 Multiple generators case

Most grids include more than one generator. The control system we analyzed in the previous paragraph is applied to each machine in the system, and the power output from each generator is added to the others to supply the load, as in Fig.1.4. Each inverter follows its own droop characteristic and, depending on its droop coefficient, gives a different amount of power. The total generated power matches the load variation and therefore stabilizes the system.

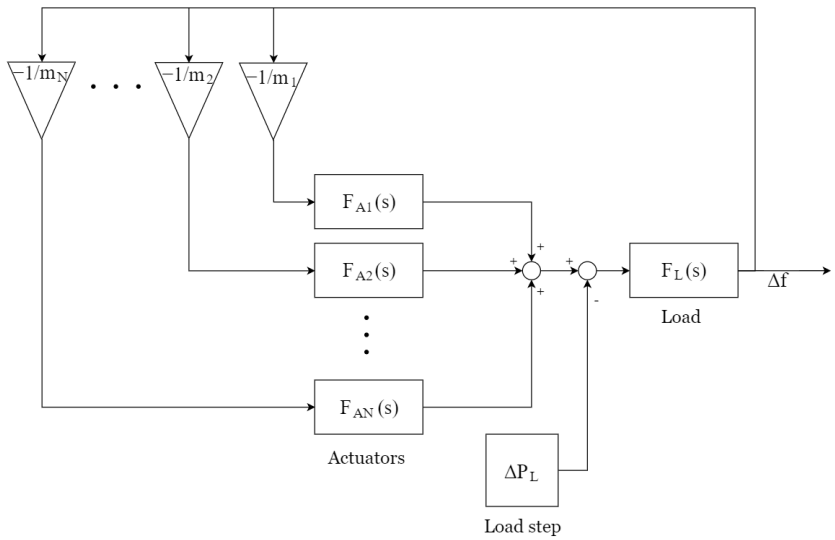

Figure 1.4: Three-generator primary regulation

1.3 Second Level (secondary control)

As we mentioned in the previous section, primary control introduces a steady-state error, which has to be corrected. This will be the target of the secondary control, which in the standard approach is carried out by a centralized architecture. This secondary level is slower than the primary one, as it zeroes the error in maximum fifteen minutes [12].

1.3.1 Steady-state behavior

Looking at the droop characteristic, we can see that by rigidly shifting the characteristic along the f-axis, we can bring the system frequency back to its nominal value. (Fig. 1.5) [9].

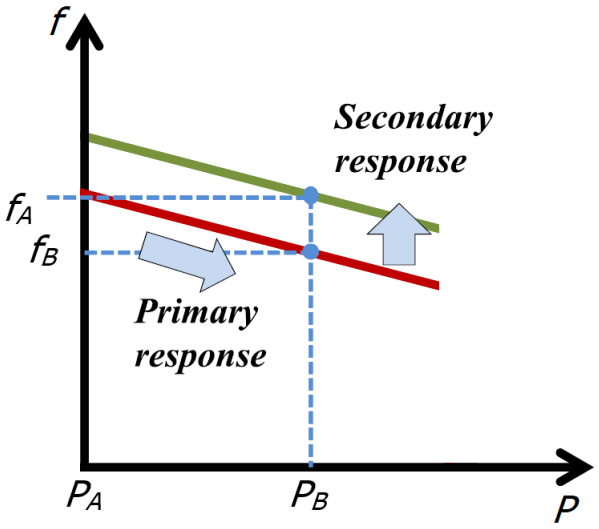

Figure 1.5: Secondary regulation working principle

1.3.2 Control scheme

With the aim of sharing the secondary regulation burden, following the approach explained in [11] we can operate by adding a control input to the one of the primary regulation, as shown in Fig. 1.6 (three generators case).

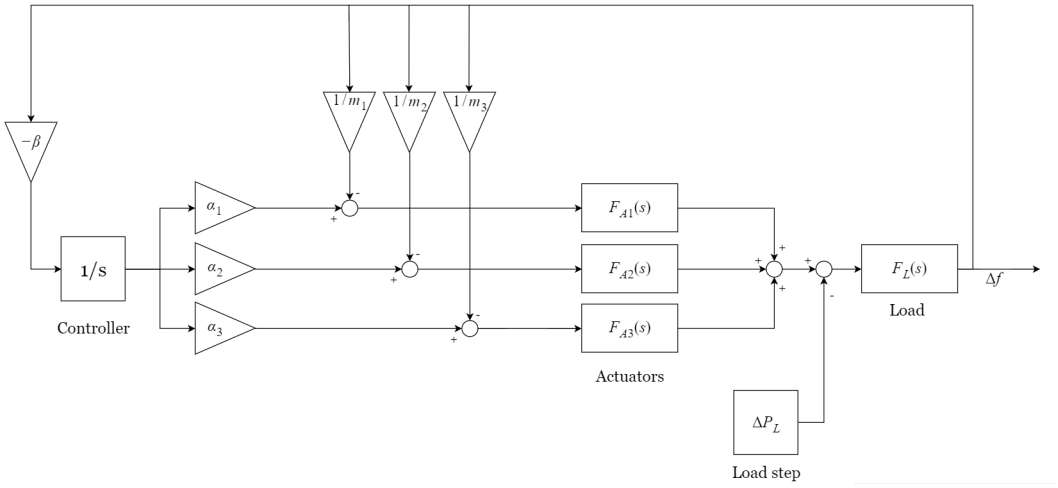

Figure 1.6: Centralized secondary control

In Figure 1.6 the feedback frequency (variation) is compared with the reference one, and the resulting error signal is integrated to bring it to zero. As we mentioned above, the output of this controller is added to the primary control input and fed to the actuator-load system. It is important to notice the centralized nature of this system: the measurement of frequency is sent to the central controller, which then sends its output signal to the DGs, where it is weighted via the coefficients α. By

varying the coefficients α (always imposing $\sum \alpha_i = 1$) we can share the load of this regulations on different generators according to the needs.

1.3.3 Problems with the traditional control scheme

The scheme we just presented does not cause problems when used in large power systems (like the ENTSO E grid), but
In the scheme we just presented some problems may arise when it is used in real situations. The main of these problems being that if one of the communication links between the central controller and the generators fail, that generator will not participate in the secondary regulation. This may not be a significant issue in large grids like the ENTSO-E, but it might have larger effects in smaller systems with fewer generators.
In order to show these effects, we have run a simulation on the scheme of Fig. 1.6, with a load step of 0.1 p.u. after 5 seconds, and $\alpha_1 = \alpha_2 = \alpha_3 = 1/3$. In Fig 1.7 we can see how the scheme works in a normal operating scenario, while in Fig 1.8 we see its behavior in case of a failure in the communication link relating to generator number 1. Notice how we reported the behavior of the variation of angular speed, which in p.u. is equal to the frequency.
It is clear how generator number 1 does not take part in the secondary regulation, as its power output variation goes to zero. This does not mean that this generator is out of service, it rather means that, after the perturbation, the generator settles down to the pre-event loading. This is an important issue to be considered, as the other two generators have to increase their power output variation (from 0.033 p.u. in the normal operating scenario to 0.05 p.u. in the faulted case) and they could experience overloading.
It is also important to highlight the fact that we simulated an inverter based system, which has a very fast dynamic response (around 20 s) compared to systems supplied by rotating machines.

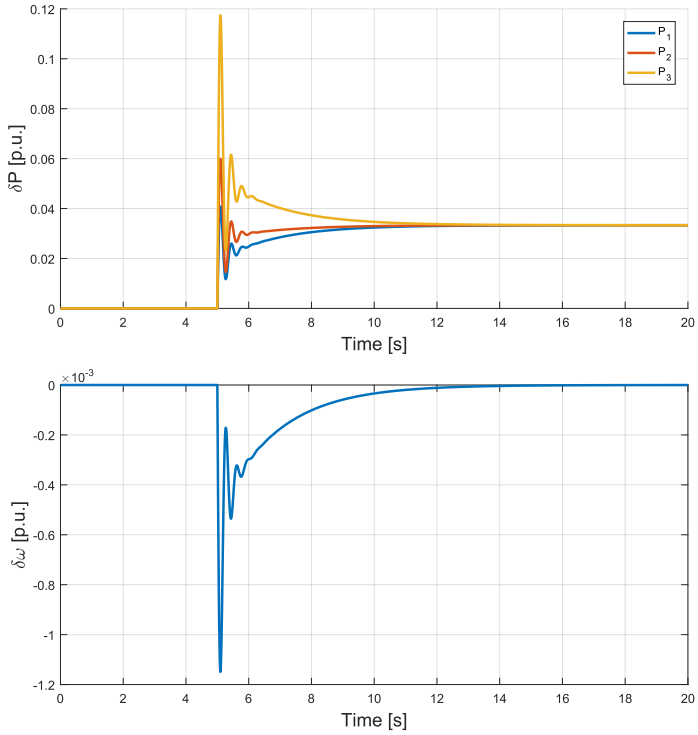

Figure 1.7: Power variations from the three generators and omega variations, normal operating scenario

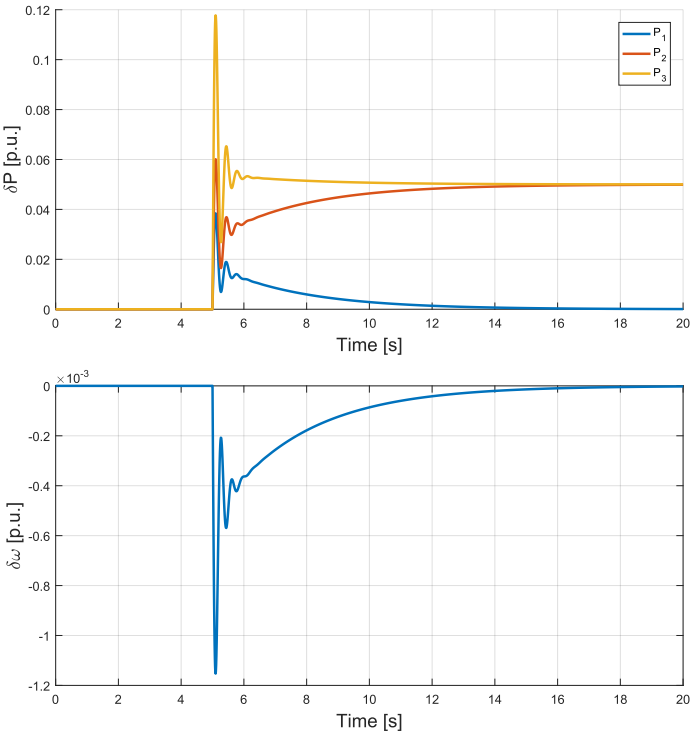

Figure 1.8: Power variations from the three generators and omega variations, fault at communication link with generator 1

Chapter 2

Distributed Control

In this chapter, we will introduce a possible solution to the problems of the centralized system, using a distributed architecture. We design a controller able to provide synchronization of the generators using information exchanged by the generators and we prove its properties using Lyapunov theorem. Finally, we provide the block scheme of the controller in a three generators case.

2.1 Introduction to distributed architectures

It is important to introduce the concept of a distributed control system. As opposed to a centralized control system, a distributed control system does not rely on the communication between a central unit (MGCC, MicroGrid Central Controller) and the Distributed Generators (DG), to operate the regulations. In our case, we want the distributed system to exploit a communication network which connects the various DG with each other and makes them exchange information between neighbors. Two DGs are called neighbors if there is a direct communication link between them. The logical scheme of these two types of structure is shown in Fig 2.1 . The distributed architecture allows the controller to operate with a sparse communication network [13]. Further in this thesis, we will show in details the robustness of this system to communication failures.

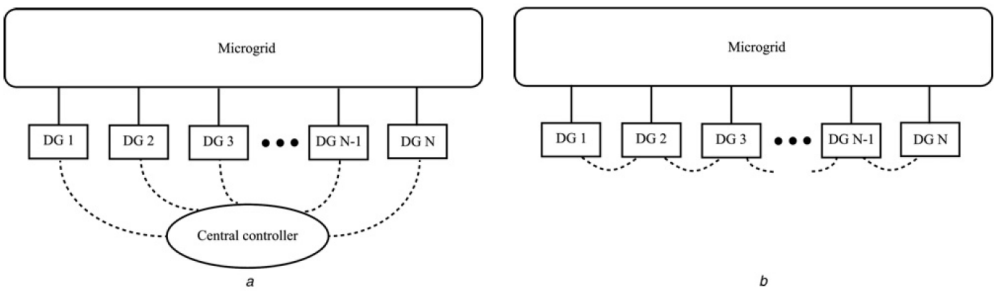

Figure 2.1: Control structures: centralized (a) and distributed (b)

2.2 Introduction to Graph theory

We will represent the communication grid between buses with a directed graph (digraph), following the approach of [14]. A digraph is usually expressed as $\mathcal{G} = (v, \varepsilon, A)$ with a set of N bus nodes $v = \{v_1, v_2, ...v_N\}$, a set of edges $\varepsilon \in v \times v$, and the associated adjacency matrix is $A = [a_{ij}] \in \mathbb{R}^{N \times N}$. An edge $(v_j, v_i) \in v$ if node i receives information from node j. a_{ij} is the weight of edge (v_j, v_i), and $a_{ij} > 0$ if $(v_j, v_i) \in v$, otherwise $a_{ij} = 0$. The set of neighbors of node i is denoted as $N_i = \{j | (v_j, v_i) \in v\}$. A digraph has a spanning tree, if there is a node i_r (called the root node), such that there is a directed path from the root node to every other node in the graph. A directed path from node i to node j is a sequence of edges. The in-degree matrix is defined as $D = diag\{d_i\}$ with $d_i = \sum_{j \in N_i} a_{ij}$. The Laplacian matrix L is defined as $L = D - A$.

In our case, there are three nodes, so A will be a 3x3 matrix with elements $a_{ij} = 1$ if node i can receive information from node j, $a_{ij} = 0$ otherwise. Notice that this means that A is not necessarily symmetric, as communication between two nodes is not always bidirectional. In our case, however, we will assume that the presence of a communication link always allows two-way information exchange, so that the adjacency matrix will always be symmetric. Another matrix we will use is the diagonal leader adjacency matrix ($G_{lead} = diag\{g_i\}$) [15], which states whether a node receives the reference frequency ω_{ref} from the leader node L ($g_i = 1$) or not ($g_i = 0$). It is important to notice that the leader node can be either one of the physical graph nodes or a virtual one, which does not belong to the graph. Examples of a three-nodes graph with virtual leader node are reported in Fig.2.2 and Fig.2.3.

$$A = \begin{bmatrix} 0 & 1 & 1 \\ 1 & 0 & 1 \\ 1 & 1 & 0 \end{bmatrix} \qquad G_{lead} = \begin{bmatrix} 1 & 0 & 0 \\ 0 & 1 & 0 \\ 0 & 0 & 1 \end{bmatrix}$$

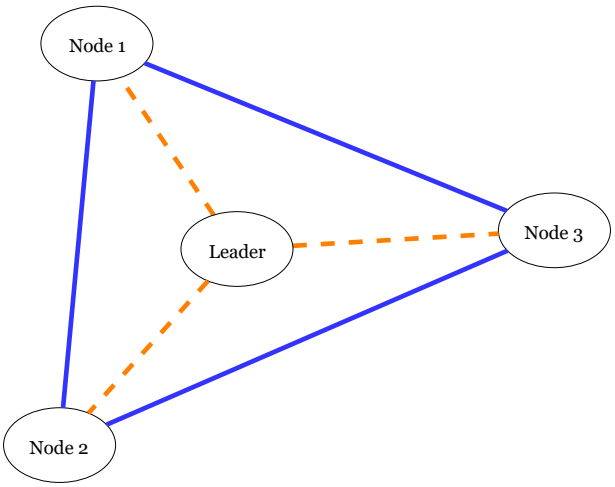

Figure 2.2: Graph example 1

$$A = \begin{bmatrix} 0 & 1 & 0 \\ 1 & 0 & 1 \\ 0 & 1 & 0 \end{bmatrix} \qquad G_{lead} = \begin{bmatrix} 1 & 0 & 0 \\ 0 & 0 & 0 \\ 0 & 0 & 1 \end{bmatrix}$$

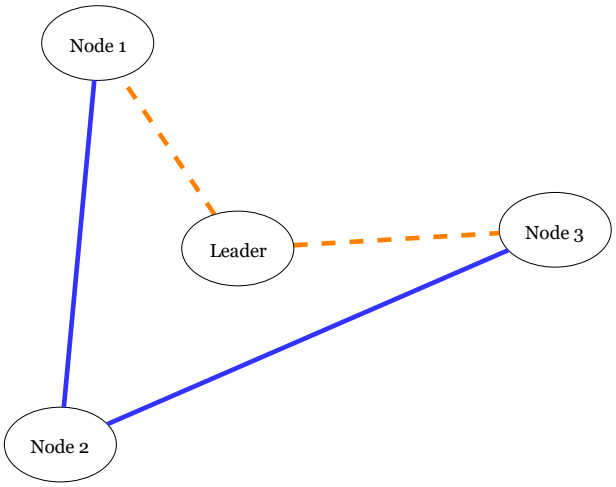

Figure 2.3: Graph Example 2

2.3 Introduction to Lyapunov theory

Lyapunov theory is a very useful tool for the study of the stability of dynamic systems. Its general concept is that, if the total energy of a system is continuously dissipated in the neighborhood of an equilibrium point, the system tends towards that equilibrium point. This means that such equilibrium point is asymptotically stable. We will use this theory to prove the stability of our controller, so it is important to recall its main aspects [16] [17].

2.3.1 Lyapunov Theorem:

Considering the following dynamic system:

$$\dot{x}(t) = \varphi(x(t)) \tag{2.1}$$

Where φ and $\dot{\varphi}$ are continuous and $\overline{x}$ is an equilibrium point, the following result holds: if we can define a function $V(x)$, called Lyapunov candidate, which is continuous (as well as its derivative), positive definite in $\overline{x}$ and such as its derivative $\dot{V}(x)$ is semidefinite negative in $\overline{x}$, which means:

$$\dot{V}(x) = \frac{dV}{dx}\frac{dx}{dt} = \frac{dV}{dx}\varphi(x) \leq 0 \, \forall \, x \in C(\overline{x}) \tag{2.2}$$

where $C(\overline{x})$ is a neighborhood of $\overline{x}$, then $\overline{x}$ is a stable equilibrium point.

Moreover, if $\dot{V}(x)$ is definite negative in $\overline{x}$, then $\overline{x}$ is an asymptotically stable equilibrium point.
So the key for this method is to find the right candidate function $V(x)$ (as there could be many of them for a given system). A typical choice is to make use of the error expression and write:

$$V(x) = e^T P e = (x - \overline{x})^T P (x - \overline{x}) \tag{2.3}$$

Where P is a definite positive matrix opportunely chosen.

2.3.2 Application to linear systems

If we consider a linear system such as:

$$\dot{x} = Ax(t) + Bu(t) \tag{2.4}$$

Lyapunov theory states that the system is asymptotically stable if and only if a matrix P (symmetric and definite positive) exists that satisfies the so-called Lyapunov equation:

$$A^T P + PA = -Q \tag{2.5}$$

For all Q symmetric and definite positive,
It is important to highlight that we will be dealing with a system defined as:

$$\dot{x} = -Ax(t) \tag{2.6}$$

Which implies that the Lyapunov equation will be:

$$A^T P + PA = Q \tag{2.7}$$

With P and Q definite positive.

2.4 Proposed distributed control system

We will operate the primary regulation through the droop method; so, for the $i-th$ bus, we can write the droop equation:

$$\omega_i = \omega_i^* - m_i \cdot (P_i - P_i^*) \tag{2.8}$$

The secondary regulation of a Microgrid, on the other hand, is a multi-agent tracking synchronization problem [18]. In these kind of problems, all agents try to synchronize their behavior to the one of a leader which acts as a command generator [19]. In our case, the DGs are the agents and they try to match their frequency to the reference

one set by the Leader Node. We will do this by adjusting the term ω_i^* (which will be the output of our controller, as in Fig.2.4), in order to shift the droop characteristic and bring the system frequency back to 50 Hz.

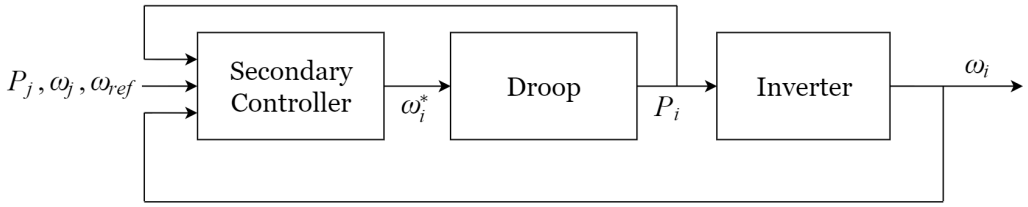

Figure 2.4: Logic scheme of the controller system

In eq. 2.9 we assigned an auxiliary control signal $u_{\omega i}$ to each DG frequency derivative.

$$\begin{cases} \dot{\omega}_1 = u_{\omega 1} \\ \dot{\omega}_2 = u_{\omega 2} \\ . \\ . \\ . \\ \dot{\omega}_N = u_{\omega N} \end{cases} \tag{2.9}$$

By differentiating eq.2.8 we can write an explicit expression of the time derivative of each frequency. This yields to eq.2.10:

$$\dot{\omega}_i = \dot{\omega}_i^* - m_i \dot{P}_i = u_{\omega i} \tag{2.10}$$

So that, solving for ω_i^*, we can write:

$$\omega_i^* = \int (u_{\omega i} + m_i \dot{P}_i) dt \tag{2.11}$$

We can now choose the nature of the auxiliary control signal $u_{\omega i}$. By exploiting the information exchanged through the communication graph $\mathcal{G}$, we can build an error signal and set:

$$u_{\omega i} = -c_\omega \cdot e_{\omega i} \tag{2.12}$$

Where $c_{\omega i}$ is a real number and $e_{\omega i}$ is the so called local neighborhood tracking error, defined as:

$$e_{\omega i} = \sum_{j \in N} a_{ij}(\omega_i - \omega_j) + g_i(\omega_i - \omega_{ref}) \tag{2.13}$$

Where a_{ij} and g_i are respectively the elements of the adjacency matrix A and leader adjacency matrix G_{lead} we introduced earlier.
Notice how this error is built for each bus with information coming both from the bus itself and neighboring buses.
We will now prove that the auxiliary control input defined in 2.12 provides frequency synchronization by using some lemmas and Lyapunov Theory. Further details on the proofs are reported in Appendix A. From 2.13 the global neighborhood error vector can be written in matrix form, as:

$$\boldsymbol{e} = (L + G_{lead})(\boldsymbol{\omega} - \boldsymbol{\omega}_{ref}) \equiv (L + G_{lead})\boldsymbol{\delta} \tag{2.14}$$

Where $\boldsymbol{\omega} = [\omega_1, \omega_2 ... \omega_N]^T$, $\boldsymbol{e} = [e_{\omega 1}, e_{\omega 2} ... e_{\omega N}]^T$ and $\boldsymbol{\omega}_{ref} = \omega_{ref} \cdot 1_N$, with 1_N the vector of ones with length N. $\boldsymbol{\delta}$ is the global disagreement vector and L is the Laplacian matrix associated with graph $\mathcal{G}$.
Lemma 1 [19]: If $\mathcal{G}$ has a spanning tree, and $g_i \neq 0$ for at least one root node, then:

$$||\boldsymbol{\delta}|| \leq ||\boldsymbol{e}||/\sigma_{min} \tag{2.15}$$

Where σ_{min} is the minimum singular value of $(L + G_{lead})$
Lemma 2 [20]: Let $\mathcal{G}$ have a spanning tree, and $g_i \neq 0$ for at least one root node. If we define a matrix $P = diag\{1/w_i\}$, where w_i are the elements of the vector $\boldsymbol{w} = B^{-1} \cdot \mathbf{1}_N$, where $B \equiv (L + G)$. Then $Q \equiv (PB + B^T P)$ is positive definite.
With this information we can prove the following theorem [18].
Theorem: Let $\mathcal{G}$ have a spanning tree, and $g_i \neq 0$ for at least one root node. If the auxiliary control $u_{\omega i}$ is chosen as in eq.2.12, then the global neighborhood error $\boldsymbol{e}$ is asymptotically stable, and so the system output frequency $\boldsymbol{\omega}$ synchronize to $\boldsymbol{\omega}_{ref}$.
Proof: using eq.2.12, we can write the expression of the global input vector:

$$\boldsymbol{u}_\omega = [u_{\omega 1}, u_{\omega 2} ... u_{\omega N}]^T = -c_\omega \boldsymbol{e} \tag{2.16}$$

We define a Lyapunov function candidate:

$$V = \frac{1}{2}\boldsymbol{e}^T P \boldsymbol{e}, \qquad P = P^T \qquad P > 0 \tag{2.17}$$

Its derivative is:

$$\dot{V} = \frac{1}{2}[\dot{\boldsymbol{e}}^T P \boldsymbol{e} + \boldsymbol{e}^T P \dot{\boldsymbol{e}}] \tag{2.18}$$

Now considering 2.12 and $\dot{\boldsymbol{\delta}} = \dot{\boldsymbol{\omega}} = -c_\omega \boldsymbol{e}$, we can see that:

$$\dot{V} = -\frac{1}{2}c_v[\boldsymbol{e}^T B^T P\boldsymbol{e} + \boldsymbol{e}^T PB\ \boldsymbol{e}] = -\frac{1}{2}c_v\boldsymbol{e}^T[B^T P + PB]\boldsymbol{e} \tag{2.19}$$

Using what we proved in Lemma 1 and Lemma 2, it is clear how, being $Q = [B^T P + PB]$ definite positive, $\dot{V}$ is definite negative and so, due to the Lyapunov Theorem [16], $\boldsymbol{e}$ is asymptotically stable. Moreover, from Lemma 1, we see that $\boldsymbol{\delta}$ is asymptotically stable, so $\boldsymbol{f}$ synchronizes to $\boldsymbol{f}_{ref}$. This completes the proof.

We can now design the second part of the control signal ω_i^* ($m_i\dot{P}_i$ in eq.2.11). Remembering that it is important to ensure that all the DGs are loaded to the same p.u. value also after the transient, and that we choose the droop coefficients based on the maximum power rating of each DG (P_{iMAX}), by imposing:

$$m_1P_1 = m_2P_2 = ... = m_NP_N \tag{2.20}$$

We can get:

$$P_1/P_{1MAX} = P_2/P_{2MAX} = ... = P_N/P_{NMAX} \tag{2.21}$$

To satisfy these equations we can define another auxiliary control signal $m_i\dot{P}_i = u_{Pi}$ and set a regulator synchronization problem:

$$\begin{cases} m_1\dot{P}_1 = u_{P1} \\ m_2\dot{P}_2 = u_{P2} \\ . \\ . \\ . \\ m_N\dot{P}_N = u_{PN} \end{cases} \tag{2.22}$$

These control inputs can be designed as in eq. 2.23. Theorem 1 can be slightly modified to show that also this variable provides the synchronization needed.

$$u_{Pi} = -c_P \cdot e_{Pi} \tag{2.23}$$

Where c_P is a real number and e_{Pi} is the so called local neighborhood tracking error, defined as:

$$e_{Pi} = \sum_{j\in N} a_{ij}(m_iP_i - m_jP_j) \tag{2.24}$$

So the total control input (from 2.11) will be:

$$\omega_i^* = \int (u_{\omega i} + u_{Pi})dt \tag{2.25}$$

Finally, we can summarize all the equations that describe the controller:

$$\begin{cases} \omega_i = \omega_i^* - m_i \cdot (P_i - P_i^*) \\ \omega_i^* = \int (u_{\omega i} + u_{Pi}) dt \\ u_{\omega i} = -c_\omega e_{\omega i} = -c_\omega [\sum_{j \in N} a_{ij}(\omega_i - \omega_j) + g_i(\omega_i - \omega_{ref})] \\ u_{Pi} = -c_P \cdot e_{Pi} = -c_P [\sum_{j \in N} a_{ij}(m_i P_i - m_j P_j)] \end{cases} \tag{2.26}$$

2.5 Control scheme

We can now use Laplace transform to build a block scheme to carry out simulations. From the transformation of eq. 2.25, we get:

$$\omega_i^*(s) = \frac{1}{s}[u_{\omega i}(s) + u_{Pi}(s)] \tag{2.27}$$

Together with the other equations in 2.26, eq.2.27 gives the control scheme of Fig.2.5, which represent the controller of one generator in a N-generator system.

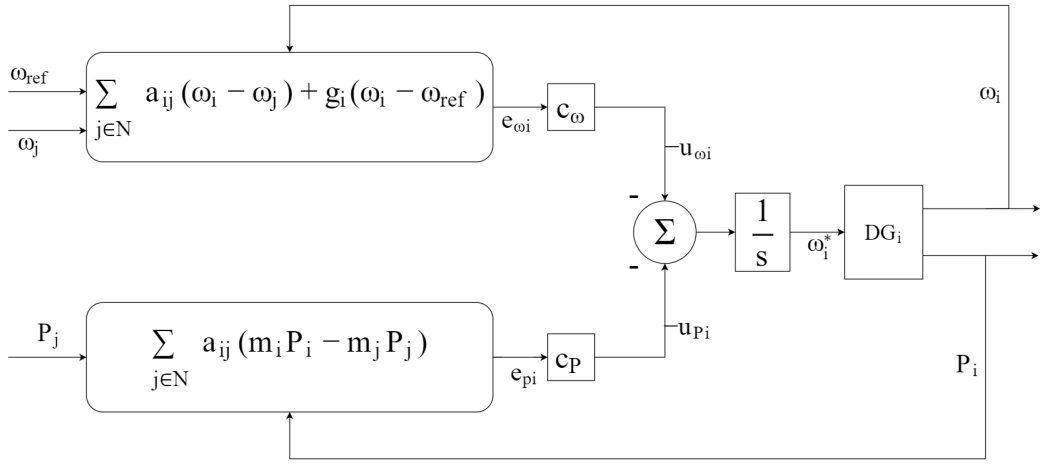

Figure 2.5: Block scheme of the controller

In Fig. 2.6, we see the Simulink scheme we realized for a grid with three DGs. In the next chapter we will analyze the behavior of this scheme in different scenarios.

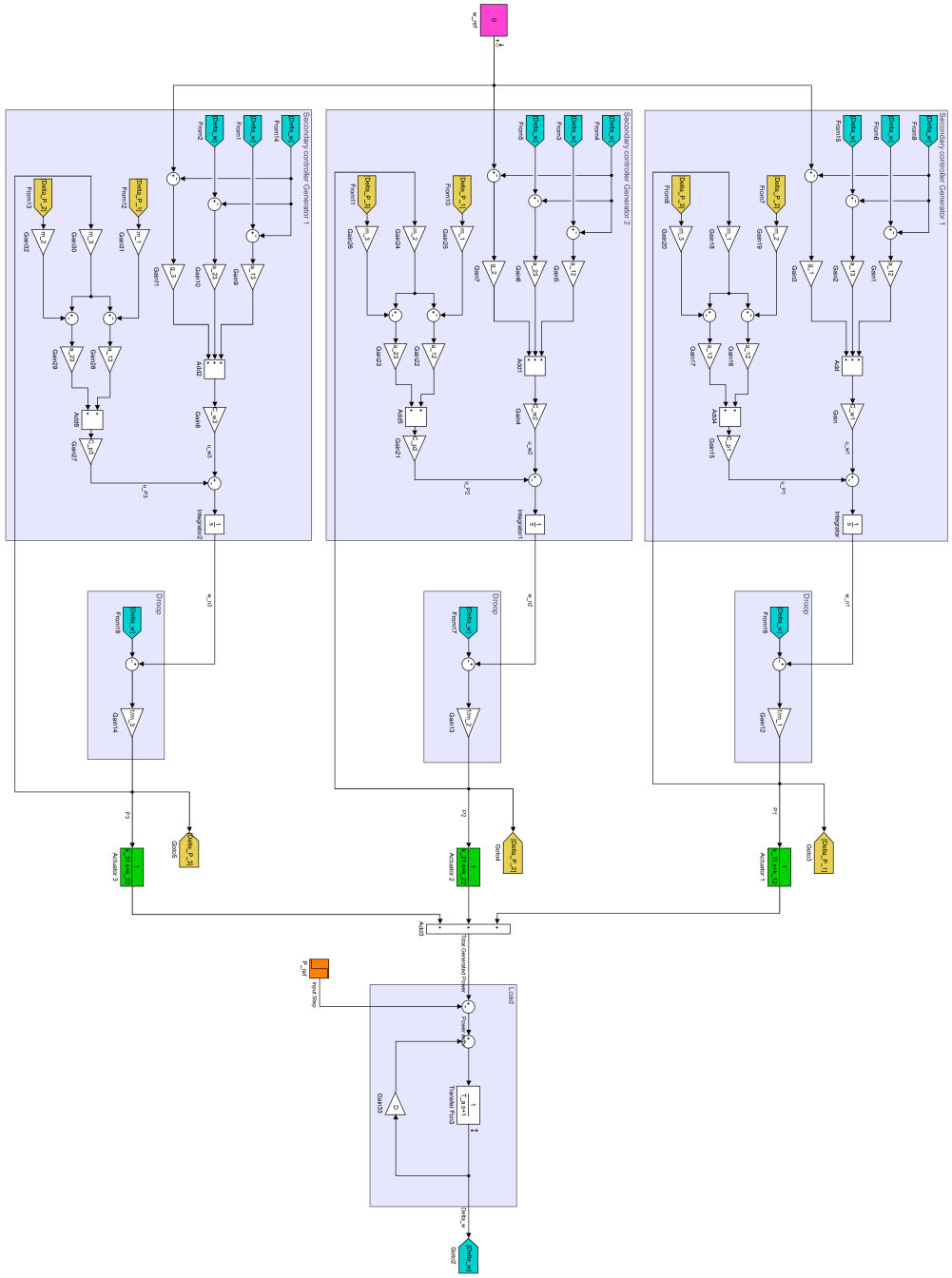

Figure 2.6: Simulink scheme for distributed controller

Chapter 3

Simulations

In this chapter, we will review the results of the simulations performed on the model explained in Chapter 2. We will describe the general parameters and data used for the simulations and we will analyze some particular cases. For every case we will show the used parameters and highlight some important graphs useful to understand the behavior of the system.

3.1 General simulation settings

We want to test the secondary regulation proprieties of our controller, so we will give as an input a step load increase of +0.1 p.u. requested power after 1 s (P_ref block), as shown in Fig.3.1. In Table 3.1 we report the set of parameters used in all of the simulations.

Table 3.1: Set of parameters used

Parameter	**Value**	**Parameter**	**Value**
c_w1	1	**k_11**	0.1
c_w2	1	**k_12**	1
c_w3	1	**k_21**	0.1
c_p1	1	**k_22**	1
c_p2	1	**k_31**	0.1
c_p3	1	**k_32**	1
m_1	3%	**T_a**	5
m_2	2%	**D**	1
m_3	1%	**w_ref**	0

Moreover, each of the operating scenarios we will analyze differs from the others for the value of the parameters regarding the communication system (a_i, g_i). In

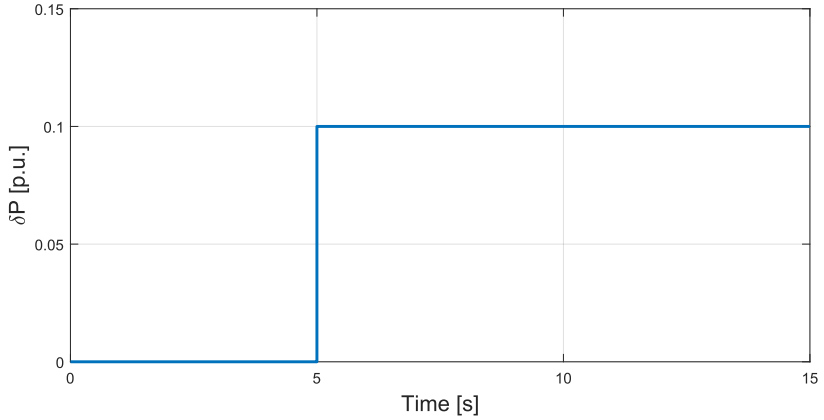

Figure 3.1: Input Step

particular, by assigning null value to any of these parameters, we are simulating the failure of a specific communication link, so that we can test the robustness of our system to communication losses. We have considered 64 possible scenarios, which cover all possible combinations of said parameters (see the table in Appendix B). Considering that many of the possible combinations represent equivalent scenarios (for example Case 2 and Case 5, which simulate the failure of communication between leader and, respectively, DG1 and DG3), we will report only one case per typology. In particular we will analyze:

- Case 1: normal operating scenario
- Case 9: single fault in the communication graph, between DG1 and DG2
- Case 25: double fault in communication graph, between DG1 and DG3, and between DG1 and DG2
- Case 57: fault of all the communication links between DGs
- Case 2: fault in communication link between DG1 and leader
- Case 4: fault in communication link between DG1 and leader, and between DG2 and leader
- Case 8: fault of all communication link between DGs and leader
- Case 10: fault of communication link between DG1 and DG2, and between DG1 and leader
- Case 26: fault of all communication links between DG1 and the rest of the network
- Case 12: failure of the communication link between DG1 and DG2, and failure of connections between leader and DG1 and DG2.

The number associated with each case identifies the operating scenario in the table of Appendix B.
For all the simulations we assumed the system to be rigid without pendular oscillations, so that all the DGs measure the same frequency ($\omega_i = \omega_j$). This assumption is common when dealing with Microgrids, as the size of the system is small.

3.2 Normal operating scenario (case 1)

This scenario represents the case in which every communication link is working. All of the communication parameters will then have value 1 (Table 3.2).

Table 3.2: Communication system parameters, normal operating scenario

Parameter	Value
g_1	1
g_2	1
g_3	1
a_12	1
a_13	1
a_23	1

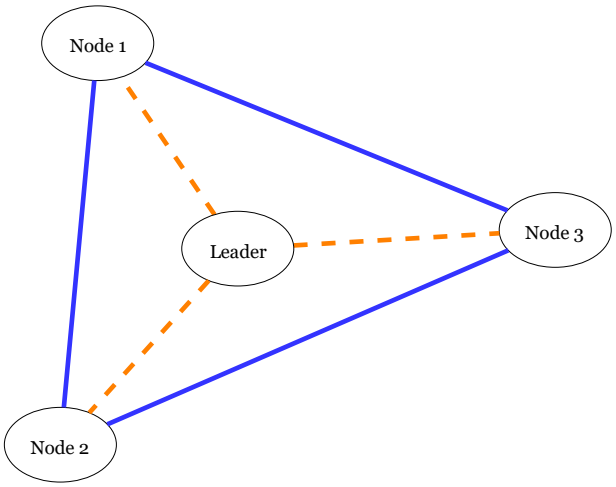

Figure 3.2: Graph case 1

In Fig.3.3a we can see how the total generated power variation converges to the input load step, this means that our controller provides primary regulation. By looking at Fig.3.3b it is also clear that the variation of power is correctly shared among the DGs based on the droop coefficients. As a matter of fact, DG1, which has $m_1 = 3\%$ gives 1.82% of load power, DG2 ($m_2 = 2\%$) gives 2.73% and DG3 ($m_3 = 1\%$) gives 5.45% power. In total they match the 10% request increase, and

the constraint $m_1P_1 = m_2P_2 = ... = m_NP_N$, which grants equal pu loading of generators is satisfied.
Moreover, from Fig.3.3c we can notice how the controller is able to perform also the secondary regulation, as the variation of omega converges to zero (which means that the output frequency matches the reference one).
Int Fig.3.3f, Fig.3.3d and Fig.3.3e we can observe the trajectories of the regulation inputs.

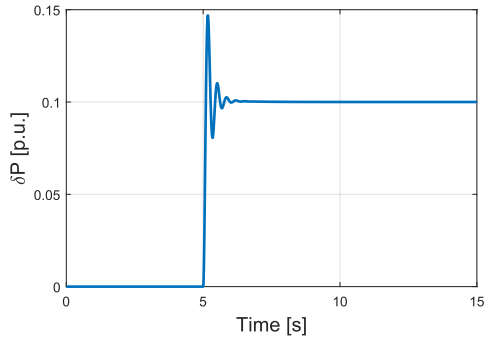

(a) Total generated power case 1

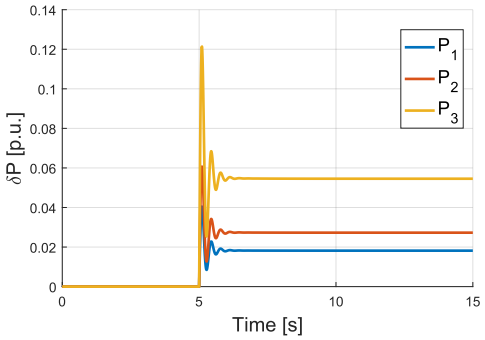

(b) Bus power case 1

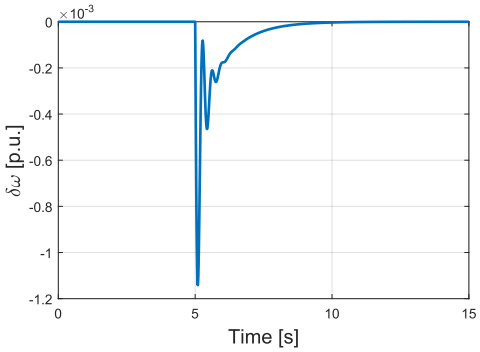

(c) Omega variation case 1

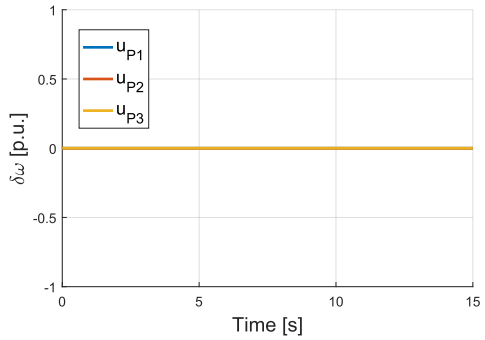

(d) u_{Pi} case 1

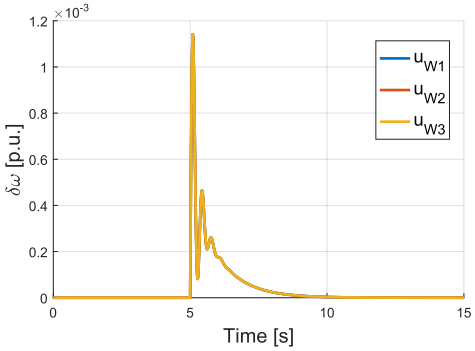

(e) $u_{\omega i}$ case 1

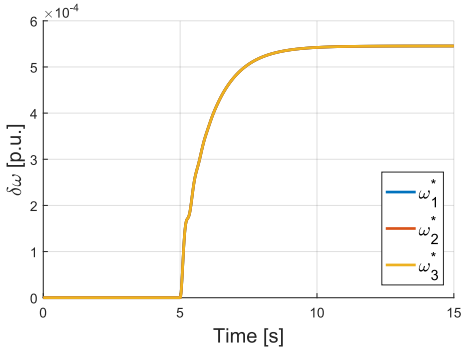

(f) Secondary regulation inputs case 1

Figure 3.3: Case 1 results

3.3 Case 9

This scenario simulates the failure of the communication link between DG1 and DG2, therefore $a_{12} = 0$ (Table 3.3). The corresponding graph is shown in Fig. 3.4.

Table 3.3: Communication system parameters, case 9

Parameter	Value
g_1	1
g_2	1
g_3	1
a_12	0
a_13	1
a_23	1

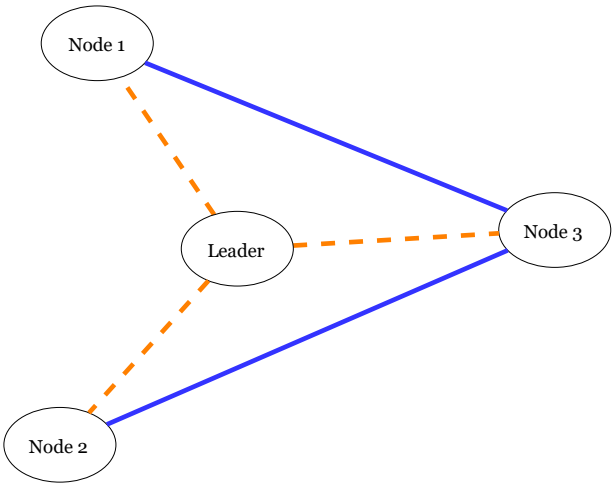

Figure 3.4: Graph case 9

As in the previous case we can see that the controller is able to provide primary regulation (see Fig.3.5a) and secondary regulation (see Fig.3.5c), as well as correct power sharing (see Fig.3.5b), despite the communication link failure.

In Fig.3.5f, Fig.3.5d and Fig.3.5e we can observe the trajectories of the regulation inputs. It is important to notice how the inputs u_{pi} remain zero for all simulation time.

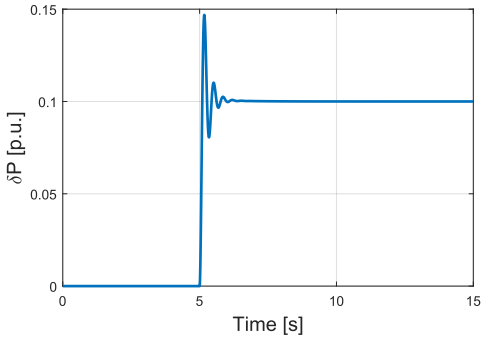

(a) Total generated power case 9

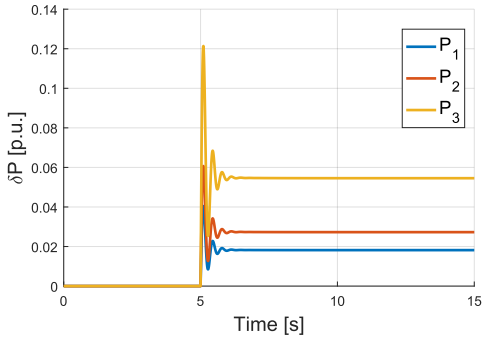

(b) Bus power case 9

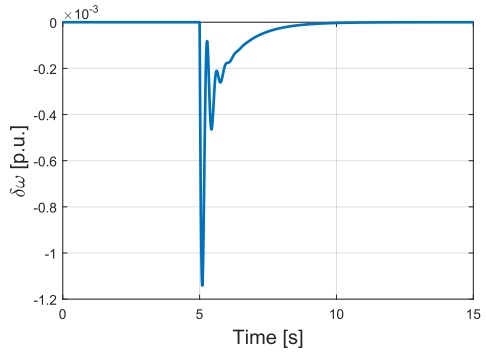

(c) Omega variation case 9

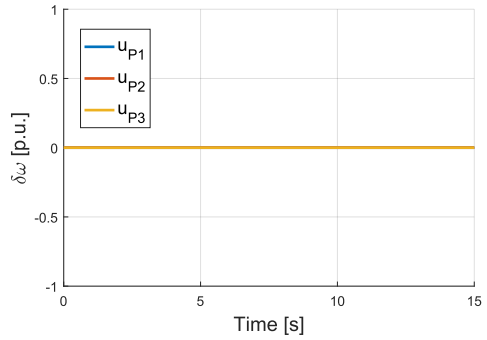

(d) u_{Pi} case 9

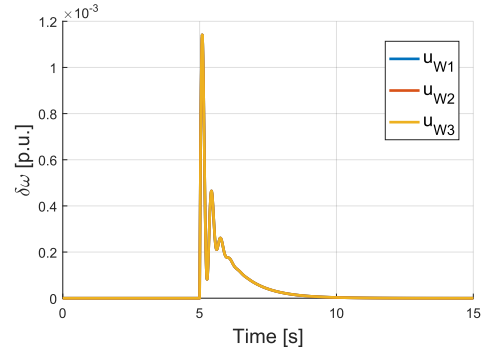

(e) $u_{\omega i}$ case 9

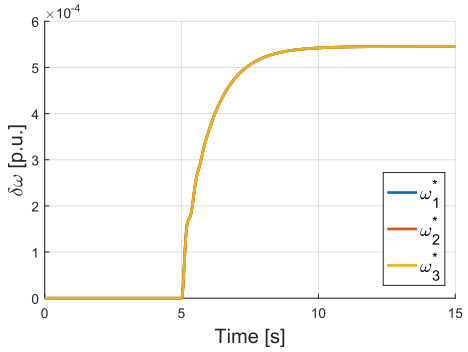

(f) Secondary regulation inputs case 9

Figure 3.5: Case 9 results

3.4 Case 25

This scenario simulates the failure of the communication links between DG1 and DG2, and between DG1 and DG3 therefore $a_{12} = a_{13} = 0$ (Table 3.4). The corresponding graph is shown in Fig. 3.6.

Table 3.4: Communication system parameters, case 25

Parameter	Value
g_1	1
g_2	1
g_3	1
a_12	0
a_13	0
a_23	1

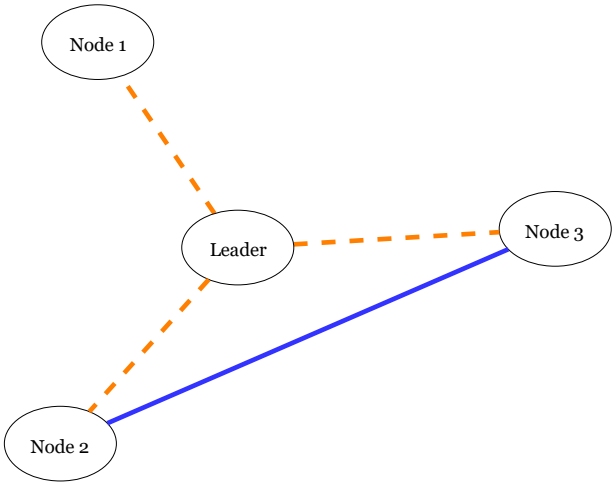

Figure 3.6: Graph example case 25

Even with a double fault, the system behaves normally and reacts correctly to the change in requested power. In Fig.3.7a and Fig.3.7c we see that primary and secondary regulations are performed. In Fig.3.7b the correct power sharing is clearly visible.

The control inputs u_{Pi} are zero throughout the simulation (Fig.3.7d) and also the other control variables (visible in Fig.3.7e and Fig.3.7f) have the same behavior of the previous cases.

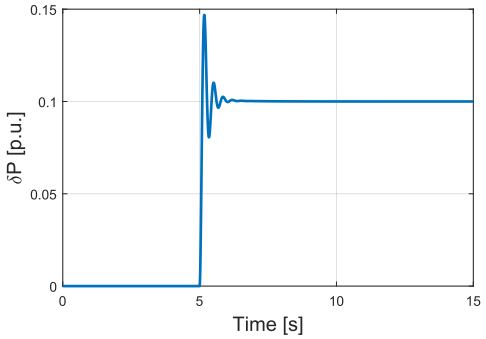

(a) Total generated power case 25

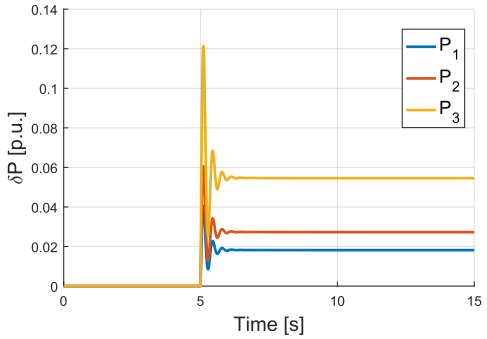

(b) Bus power case 25

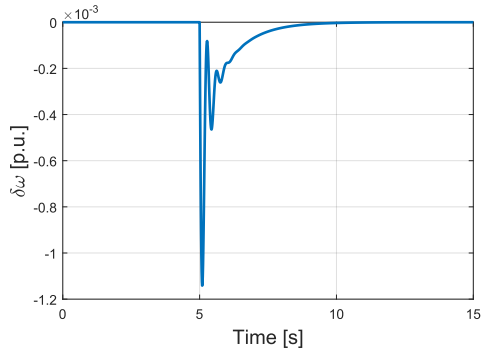

(c) Omega variation case 25

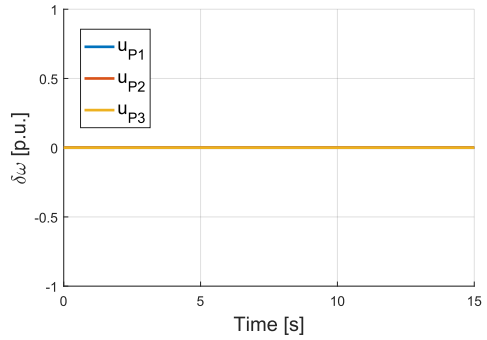

(d) u_{Pi} case 25

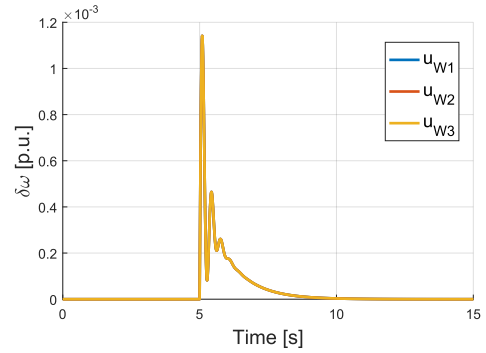

(e) $u_{\omega i}$ case 25

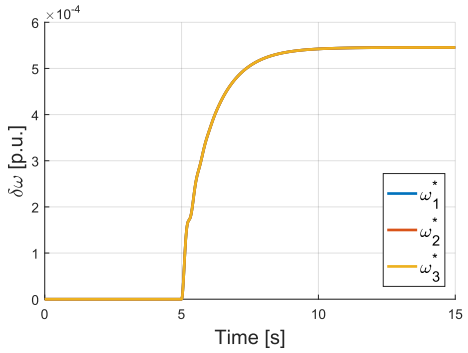

(f) Secondary regulation inputs case 25

Figure 3.7: Case 25 results

3.5 Case 57

This scenario simulates the failure of all the communication links between the DGs, therefore $a_{12} = a_{13} = a_{23} = 0$ (Table 3.5). The corresponding graph is shown in Fig.3.6.

Table 3.5: Communication system parameters, case 57

Parameter	Value
g_1	1
g_2	1
g_3	1
a_12	0
a_13	0
a_23	0

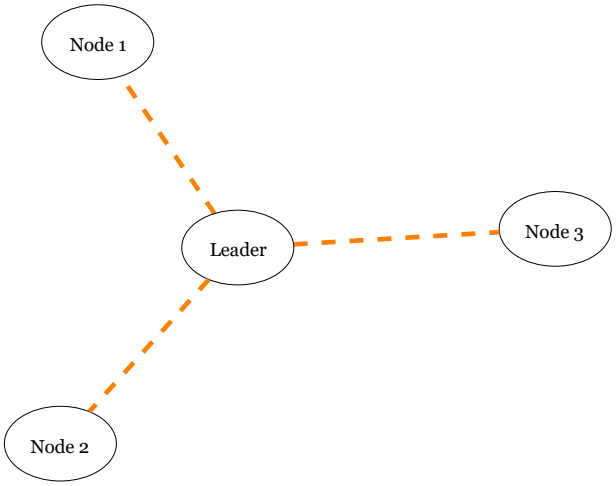

Figure 3.8: Graph case 57

Once more, even with a triple fault, the system behaves normally and reacts correctly to the change in requested power. In Fig.3.9a and Fig.3.9c we see that primary and secondary regulations are performed. In Fig.3.9b the correct power sharing is clearly visible.

The control inputs u_{Pi} are zero throughout the simulation (Fig.3.9d) and also the other control variables (visible in Fig.3.9e and Fig.3.9f) have the same behavior of the previous cases.

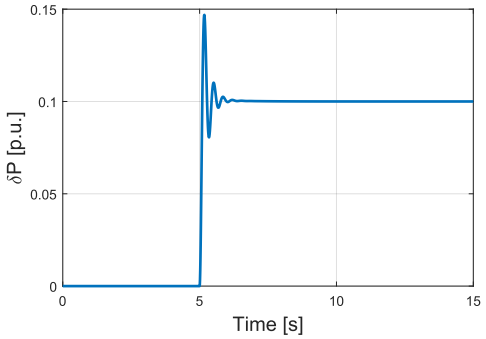

(a) Total generated power case 57

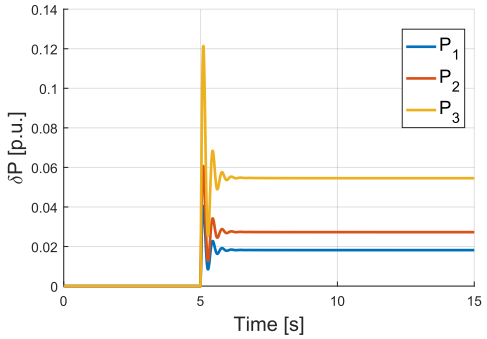

(b) Bus power case 57

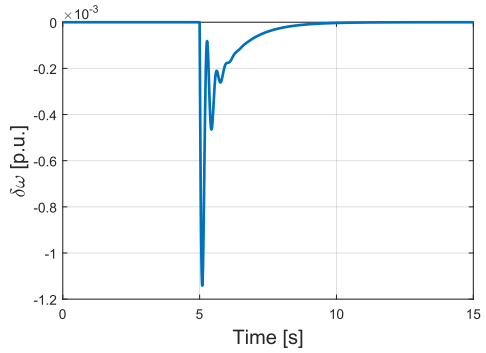

(c) Omega variation case 57

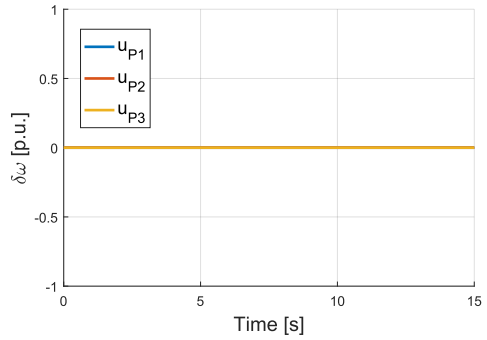

(d) u_{Pi} case 57

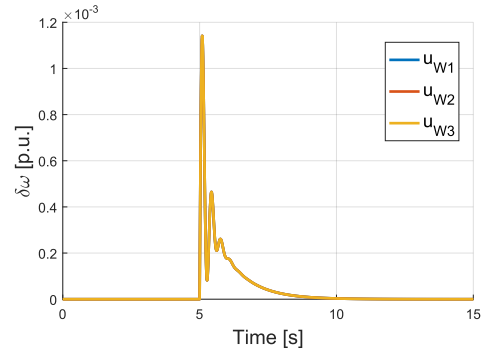

(e) $u_{\omega i}$ case 57

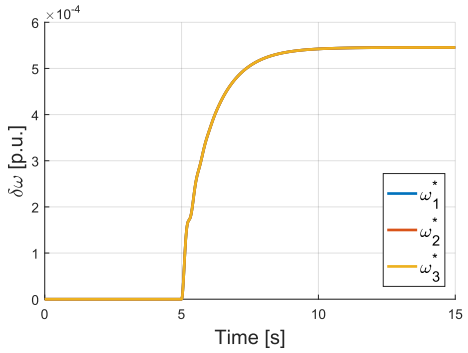

(f) Secondary regulation inputs case 57

Figure 3.9: Case 57 results

3.6 Case 2

This scenario simulates the failure of the communication link between the Leader node and DG1, therefore $g_1 = 0$ (Table 3.6) . The corresponding graph is shown in Fig.3.10.

Table 3.6: Communication system parameters, case 2

Parameter	Value
g_1	0
g_2	1
g_3	1
a_12	1
a_13	1
a_23	1

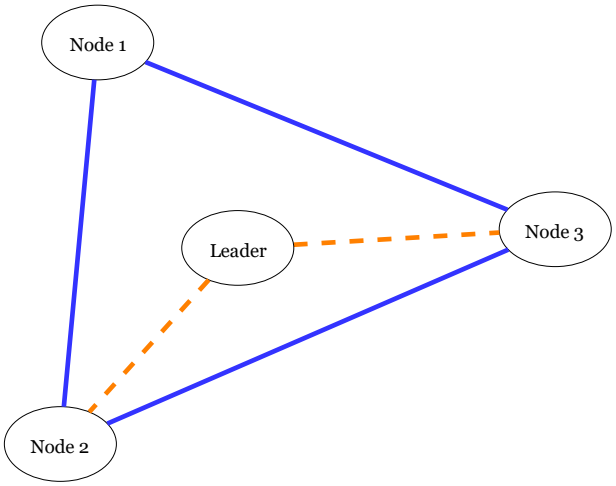

Figure 3.10: Graph case 2

We can see from Fig.3.11a that the controller performs the primary regulation, and from Fig.3.11b we also observe that the power load variation is shared correctly. This last point is very important, it shows how this system allows a DG to work correctly even if it doesn't get the reference from the Leader. It is a significant improvement from the centralized system, where DGs isolated from the central controller couldn't contribute to the regulations.

In this case it is interesting to look at the behavior of the control inputs. In Fig.3.11d, Fig.3.11e and Fig.3.11f it is clear how the control inputs relative to DG1 are different from the other two, and in particular $u_{p1} = 0$.

It is possible to notice that the dynamics of the variations of frequency are slower than the previous cases (transient ends in approximately 10 seconds, while previously it was 5 seconds).

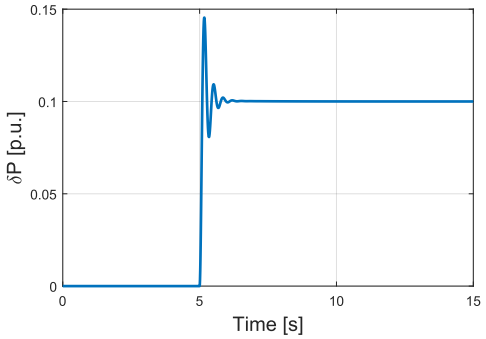

(a) Total generated power case 2

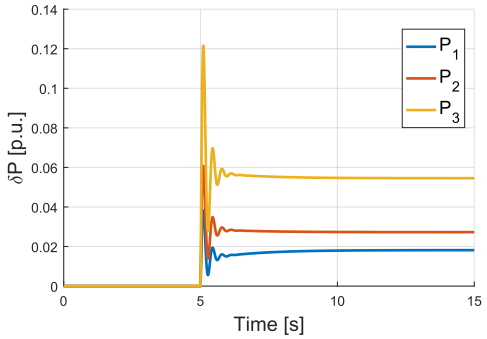

(b) Bus power case 2

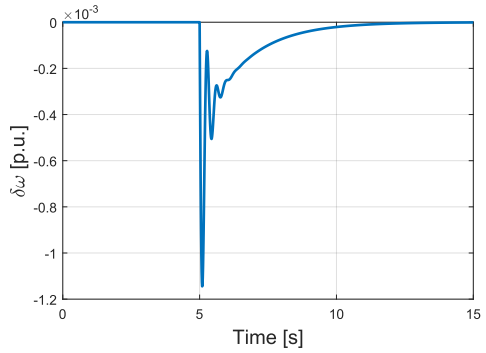

(c) Omega variation case 2

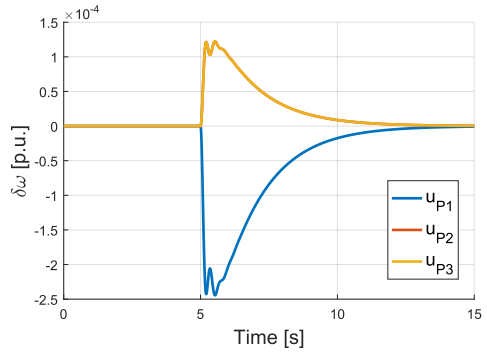

(d) u_{Pi} case 2

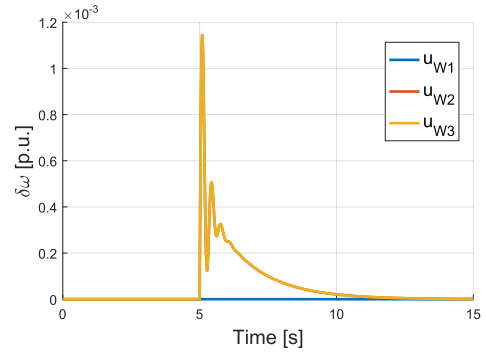

(e) $u_{\omega i}$ case 2

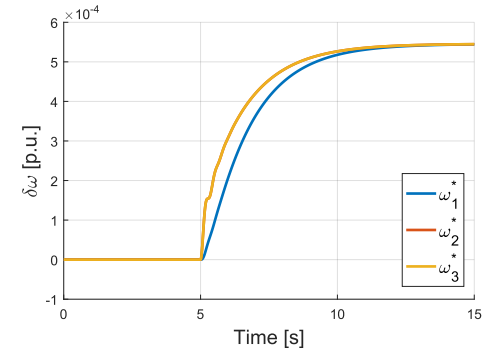

(f) Secondary regulation inputs case 2

Figure 3.11: Case 2 results

3.7 Case 4

This scenario simulates the failure of the communication link between the Leader node and both DG1 and DG2, therefore $g_1 = g_2 = 0$ (Table 3.7). The corresponding graph is shown in Fig. 3.10.

Table 3.7: Communication system parameters, case 4

Parameter	Value
g_1	0
g_2	0
g_3	1
a_12	1
a_13	1
a_23	1

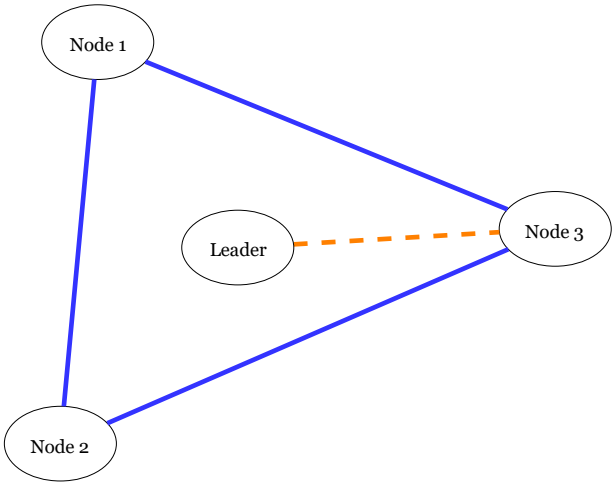

Figure 3.12: Graph case 4

In this case, the dynamics are even slower than the previous case, as the transient lasts around 15 seconds (see Fig.3.13c), but still in an acceptable range. Despite the loss of communication between the leader and two of the DGs, the system is still able to provide primary and secondary regulation, and correct power sharing, as we can observe in Fig. 3.13a and Fig.3.13b.

In Fig.3.13d, Fig.3.13e and Fig.3.13f we can see that the control inputs of DG1 and DG2 have the same trajectory, as they are both unconnected to the leader.

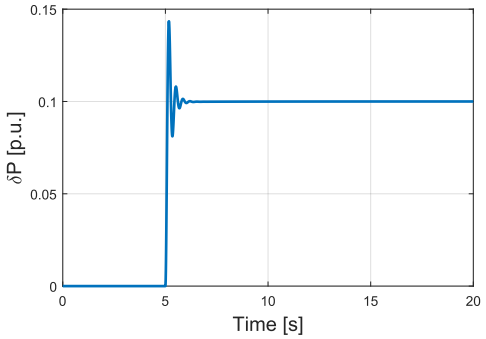

(a) Total generated power case 4

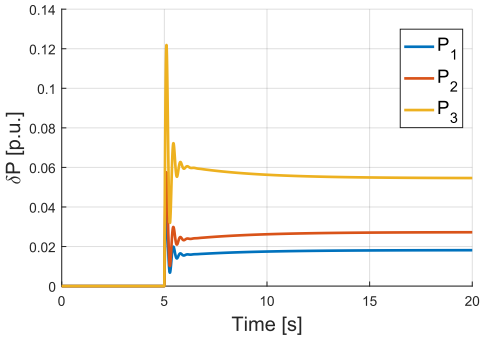

(b) Bus power case 4

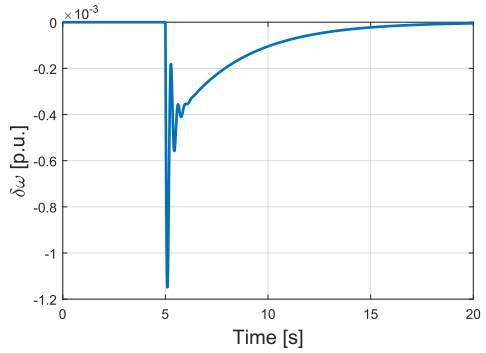

(c) Omega variation case 4

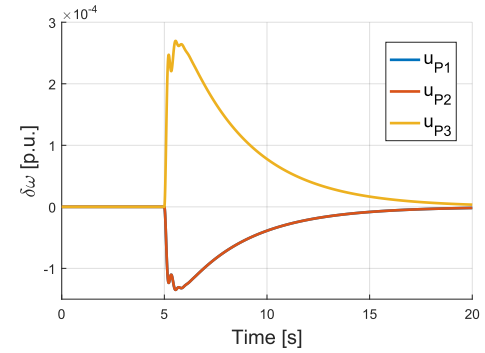

(d) u_{Pi} case 4

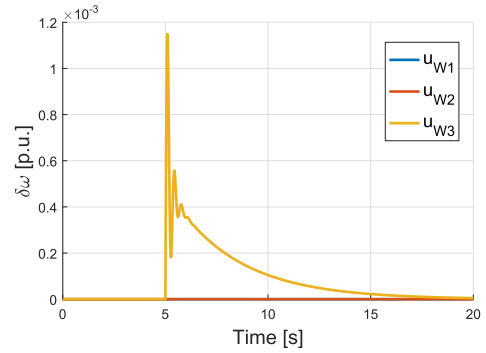

(e) $u_{\omega i}$ case 4

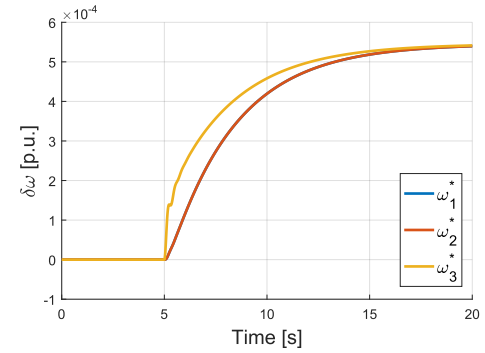

(f) Secondary regulation inputs case 4

Figure 3.13: Case 4 results

3.8 Case 8

This scenario simulates the failure of all the communication links between the Leader node and the DGs, therefore $g_1 = g_2 = g_3 = 0$ (Table 3.8). The corresponding graph is shown in Fig.3.14.

Table 3.8: Communication system parameters, case 8

Parameter	Value
g_1	0
g_2	0
g_3	0
a_12	1
a_13	1
a_23	1

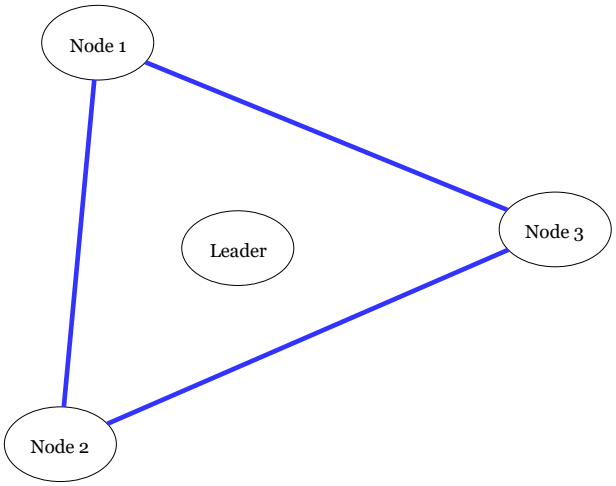

Figure 3.14: Graph case 8

In this case, there is a lack of reference in the system, as no DG has a connection to the leader. The controller is unable to provide secondary regulation, as we can see in Fig.3.15c, where $\delta\omega$ clearly shows a non-zero steady-state error. Moreover, all the secondary regulation inputs are null, as we can see in Fig.3.15d, Fig.3.15e and Fig.3.15f. Primary regulation, on the other hand, being independent on the communication system, is performed correctly, as power request is correctly balanced by power generation (see Fig.3.15a and Fig.3.15b).

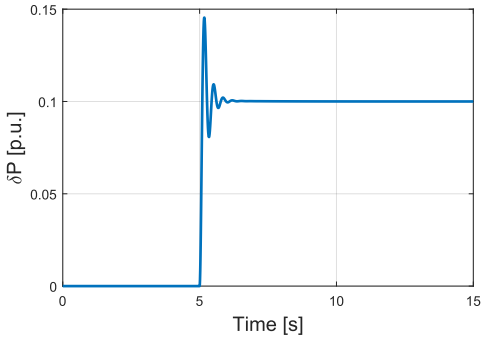

(a) Total generated power case 8

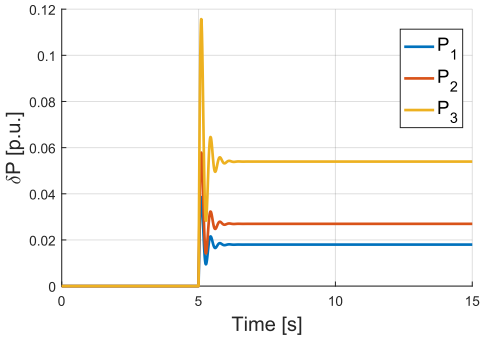

(b) Bus power case 8

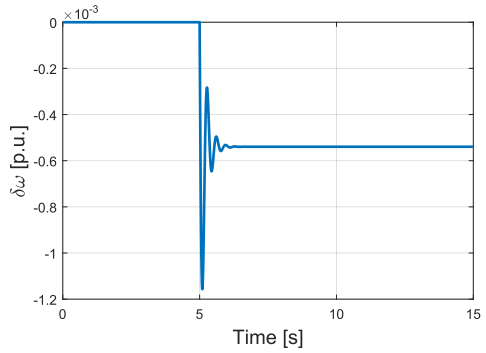

(c) Omega variation case 8

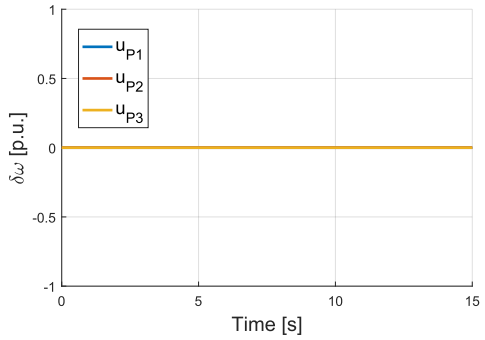

(d) u_{Pi} case 8

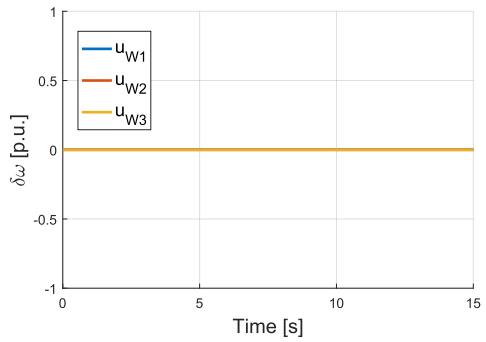

(e) $u_{\omega i}$ case 8

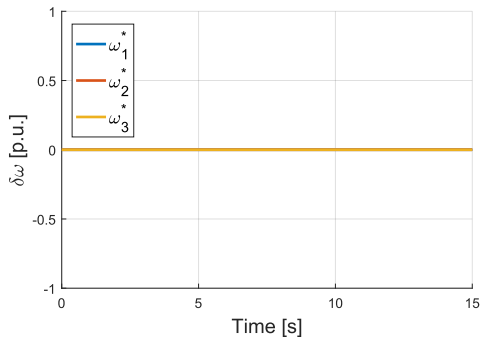

(f) Secondary regulation inputs case 8

Figure 3.15: Case 8 results

3.9 Case 10

This scenario simulates the failure of communication link between the Leader node and DG1, and between DG1 and DG2, therefore $g_1 = 0$ and $a_{12} = 0$ (Table 3.9). The corresponding graph is shown in Fig.3.16.

Table 3.9: Communication system parameters, case 10

Parameter	Value
g_1	0
g_2	1
g_3	1
a_12	0
a_13	1
a_23	1

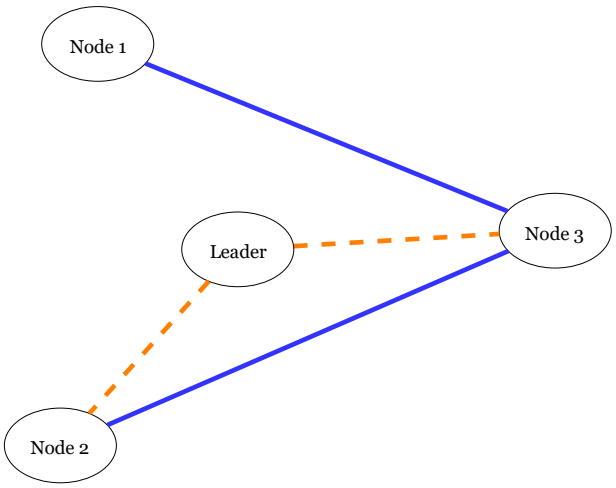

Figure 3.16: Graph case 10

In this case the system is able to provide primary and secondary regulation (Fig.3.17a and Fig.3.17c), as well as correct power sharing (see Fig.3.17b).

In Fig.3.17f, Fig.3.17d and Fig.3.17e we can observe the trajectories of the regulation inputs.

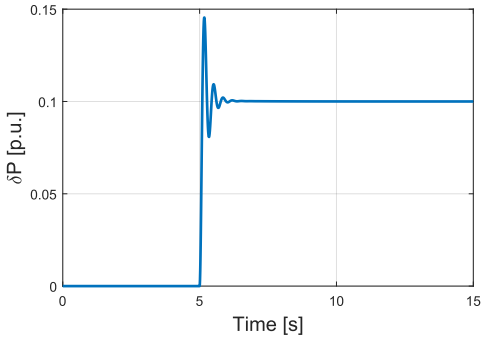

(a) Total generated power case 10

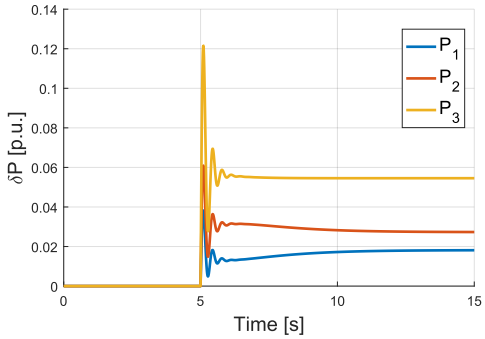

(b) Bus power case 10

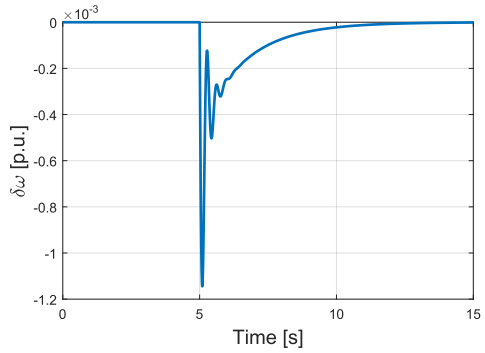

(c) Omega variation case 10

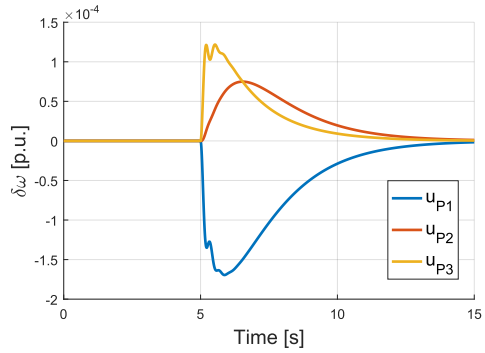

(d) u_{Pi} case 10

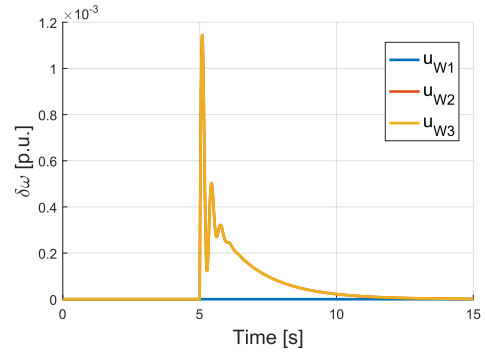

(e) $u_{\omega i}$ case 10

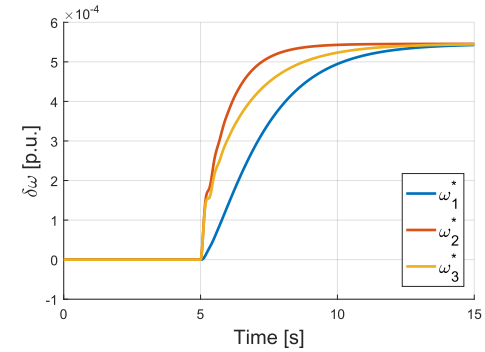

(f) Secondary regulation inputs case 10

Figure 3.17: Case 10 results

3.10 Case 26

In this case DG1 is completely isolated from the rest of the communication system, therefore $g_1 = 0$ and $a_{12} = a_{13} = 0$ (Table 3.10). The corresponding graph is shown in Fig.3.18.

Table 3.10: Communication system parameters, case 26

Parameter	Value
g_1	0
g_2	1
g_3	1
a_12	0
a_13	0
a_23	1

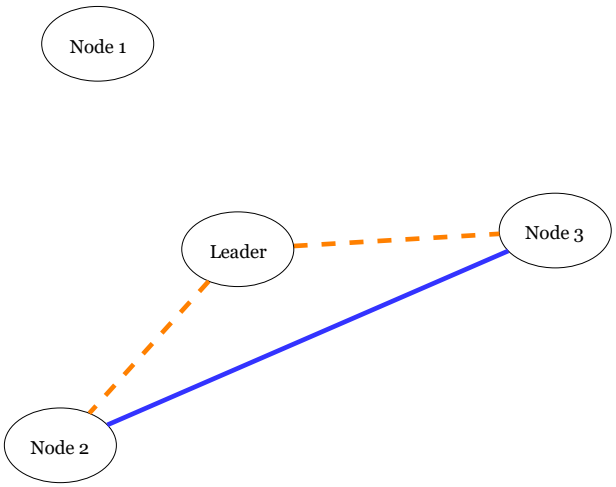

Figure 3.18: Graph case 26

Being isolated from the rest of the system, DG1 doesn't receive the reference, and so it doesn't contribute to the secondary regulation. As we can see in Fig.3.19f, Fig.3.19d and Fig.3.19e its regulation variables and input are zero, and this causes its generated power variation (Fig.3.19b, $P1$) to go to zero. This means that DG1 goes back to the pre-load variation power output and does not participate in the secondary control. The system is overall able to perform both primary and secondary regulation (see Fig.3.19a and Fig.3.19c), but without the contribution of DG1 we have the risk of overloading the other DGs. We can see how this situation is similar to the one we simulated in Chapter 1 (Fig.1.8) with the centralized controller and has similar results. With the distributed controller, however, three faults were needed to take down one DG, while with the centralized controller only a single fault was enough.

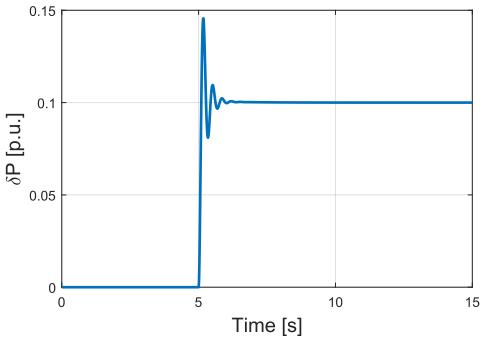

(a) Total generated power case 26

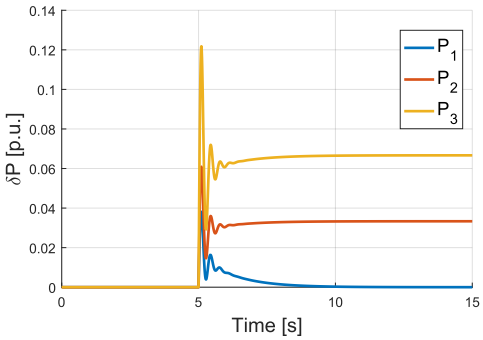

(b) Bus power case 26

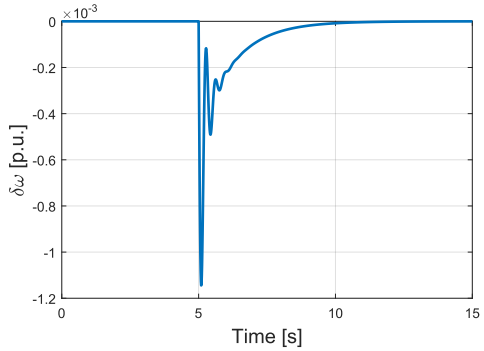

(c) Omega variation case 26

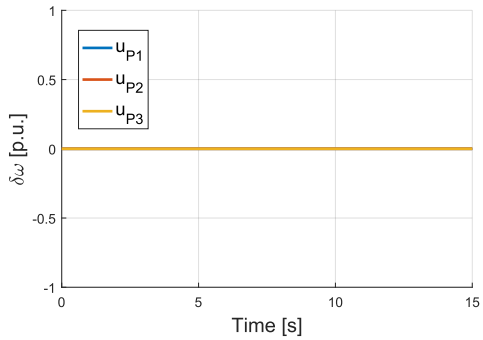

(d) u_{Pi} case 26

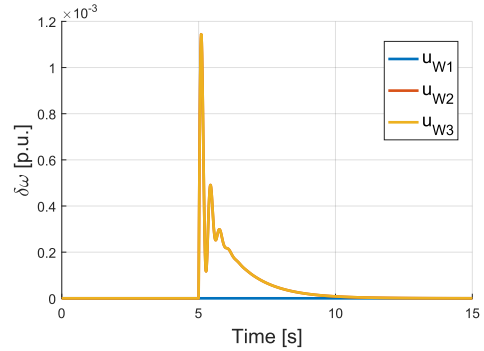

(e) $u_{\omega i}$ case 26

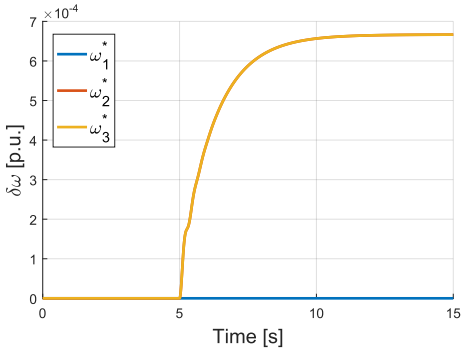

(f) Secondary regulation inputs case 26

Figure 3.19: Case 26 results

In Fig.3.20a and Fig.3.20b we show the behavior of the system after a load step of 0.2 p.u. and imposing a power output limit for DG2 (5% of the load) and DG3 (10% of the load). This situation could occur, for example, in a system where DG2 and DG3 are inverters of battery energy storage systems (BESS), in case of a cooling system fault. The safety system would set a limit to the power output of the inverters.

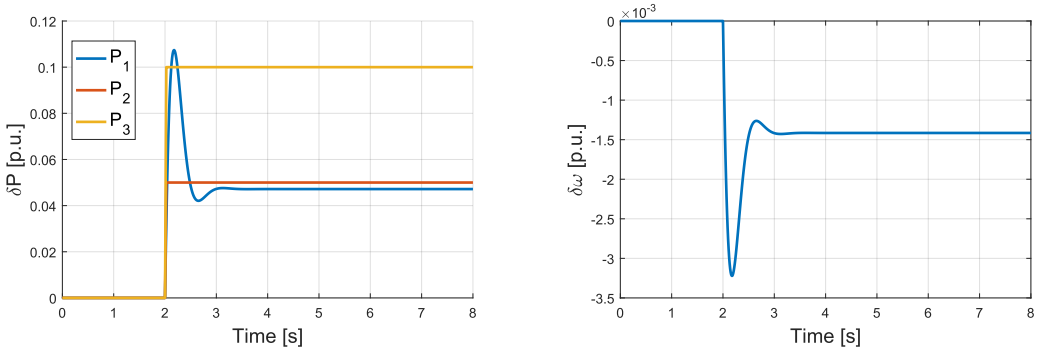

(a) Bus power case 26 with saturation

(b) Omega variation case 26 with saturation

Figure 3.20: Case 26 results with saturation

We can see that the system is not able to bring the frequency variation to zero, but it is still stable, as it reaches steady state. When DG2 and DG3 reach their respective saturation limit, DG1 is still working following its droop characteristic, so it is able to supply to the load variation needed to stop the frequency transient.

3.11 Case 12

This configuration is constituted by a spanning tree in the graph, and one single connection between the leader and one of the root nodes of the graph. As we proved in Chapter 2, this is the minimum number of connection which allows the controller to perform correctly. The corresponding graph is shown in Fig.3.21.

Table 3.11: Communication system parameters, case 12,

Parameter	Value
g_1	0
g_2	0
g_3	1
a_12	0
a_13	1
a_23	1

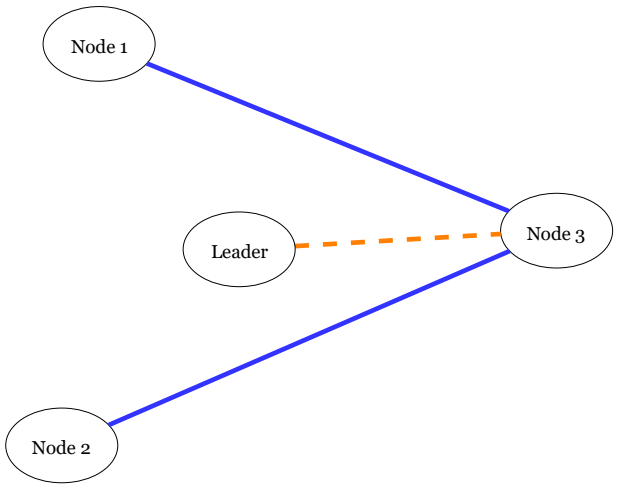

Figure 3.21: Graph case 12

By looking at the various figures, we see, as expected, that the system provides primary and secondary regulation (see Fig.3.22a, Fig. and Fig.3.22b), as well as power sharing (see Fig.3.22b). The behaviors of the control variables are reported in Fig.3.22f, Fig.3.22d and Fig.3.22e.

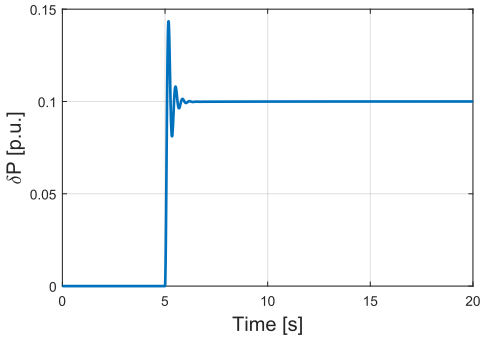

(a) Total generated power case 12

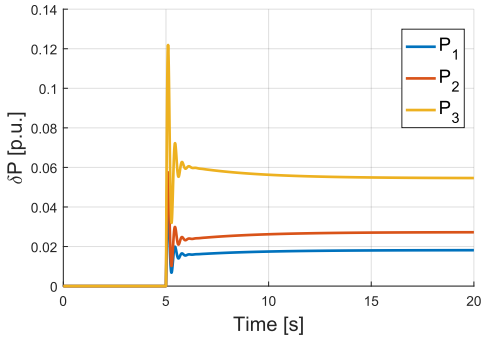

(b) Bus power case 12

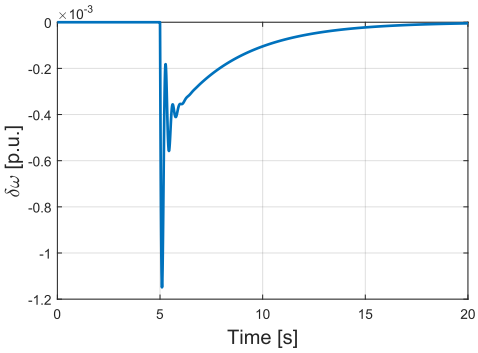

(c) Omega variation case 12

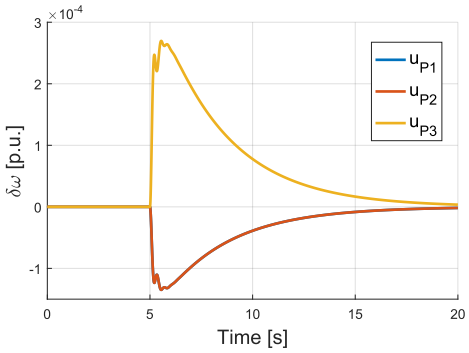

(d) u_{Pi} case 12

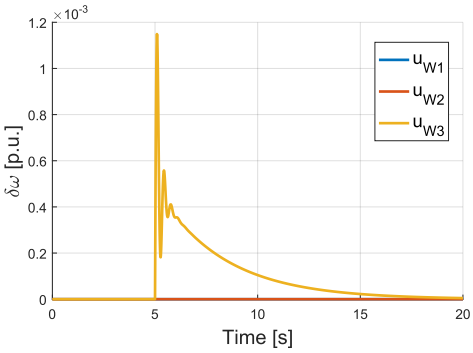

(e) $u_{\omega i}$ case 12

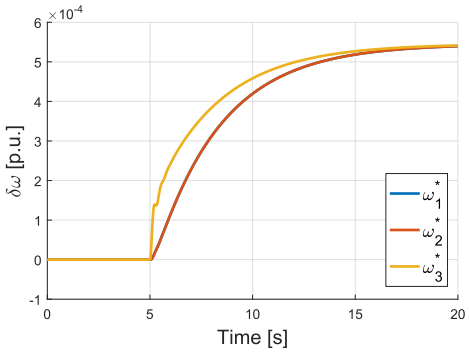

(f) Secondary regulation inputs case 12

Figure 3.22: Case 12 results

3.12 Conclusions

Before commenting on the simulation results, we have to make an important observation on the two auxiliary control input u_ω and u_P. We report their expressions in eq.3.1 and eq.3.2

$$u_{\omega i} = -c_\omega e_{\omega i} = -c_\omega [\sum_{j \in N} a_{ij}(\omega_i - \omega_j) + g_i(\omega_i - \omega_{ref})] \tag{3.1}$$

$$u_{Pi} = -c_P \cdot e_{Pi} = -c_P [\sum_{j \in N} a_{ij}(m_i P_i - m_j P_j)] \tag{3.2}$$

Looking at the expression of $u_{\omega i}$, and remembering the assumption of rigid system ($\omega_i = \omega_j$) we made earlier, we can see how, in our case, the element $a_{ij}(\omega_i - \omega_j)$ is always equal to zero. $u_{\omega i}$ is in practice an error signal built with information coming from the leader of our system and the local generator, without contributions from neighboring DGs. By looking at the expression of u_{Pi}, instead, we see that it is a signal also built with contributions from the other generators, as the term $\sum_{j \in N} a_{ij}(m_i P_i - m_j P_j)$ is not always zero. We can now proceed and further analyze the results of our simulations.

In cases 9, 25 and 57, which are the ones where we observe the behavior of the system after a communication failure between two of the DGs ($a_i j = 0$), we can see how the u_{Pi} are always equal to zero, while the $u_{\omega i}$ are non-zero. This means that the system, when all the DGs receive the reference from the leader, acts as a centralized one, and does not exploit the communication links between the DGs. The system, therefore, is not influenced by any change of this graph.

In cases 2 and 4, in which we test the behavior of the system after a failure in the communication between leader and DGs ($g_i = 0$), we can see how the generator directly affected by the fault has u_ω equal to zero, and all of the generators have a non-zero u_P. This behaviour shows how the communication graph between DGs acts as a sort of backup to the direct link with the leader, as it starts operating when a direct link fails.

In general, after seeing the various simulation results, we can state that the system we designed based on the communication between distributed generators is more robust to communication failures than the centralized one.

Chapter 4

Study case: the grid of Anjouan, Comores

Engie-EPS is in charge of revamping the grid on the island of Anjouan since early 2018. This project constitutes the case study in which we applied the controller we developed in Chapter 2. In this chapter, we will present the main features of the grid and the ways we realized them in DIgSILENT PowerFactory, as well as the main aspects of Engie-EPS project. We will also highlight some of the issues we had to address while designing the system and the advantages the project will bring to Anjouan.

4.1 The Island

The Union of Comoros is a country composed of three main islands and many smaller ones, and it is located in the Mozambique channel (Indian Ocean), close to the north-western part of Madagascar. Anjouan is a volcanic, triangular shaped island and with its 424 square kilometers area it is the second largest island of the archipelago. Its central part is mountainous and covered by tropical forests, therefore most of the 277.000 inhabitants live on the coasts. Mutsamoudou is the chief town and has the largest commercial harbor of the island. In Fig.4.1 we can see the topographic map of Anjouan.

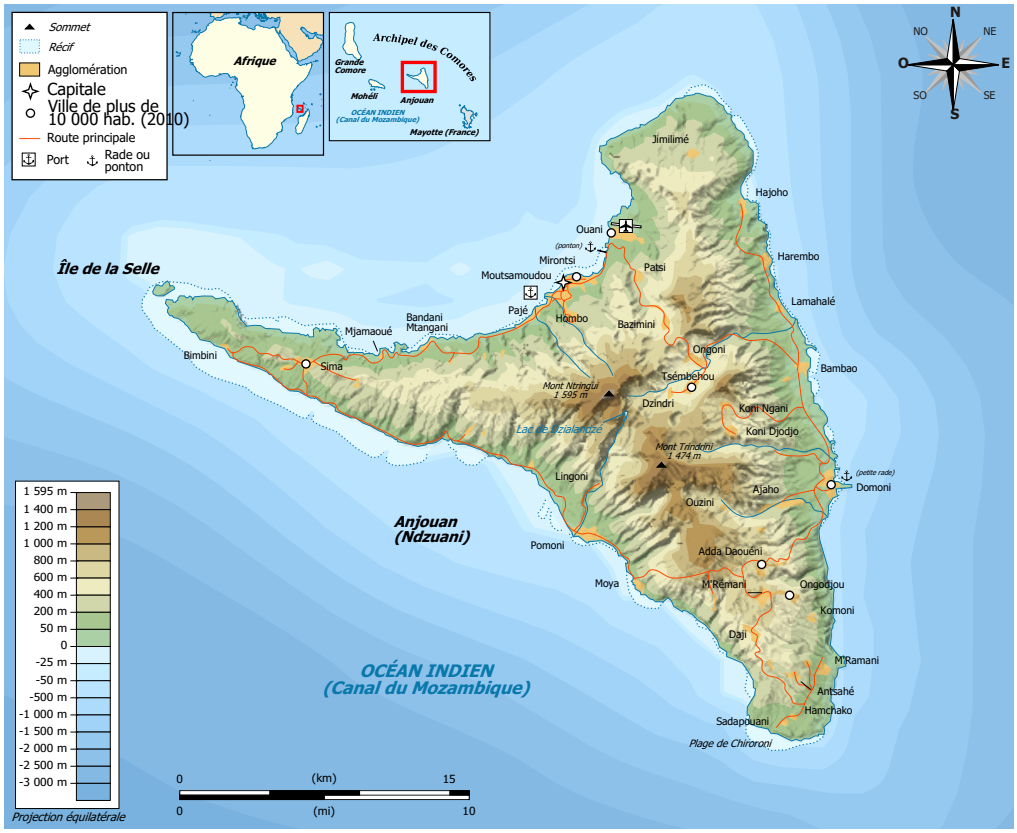

Figure 4.1: Topographic map of Anjouan

4.2 Grid Overview

4.2.1 Generators

The grid is supplied entirely by an array of nine low voltage ($0.4\,kV$) Diesel generators, located in Trenani (close to Patsi in Fig4.1). Out of these nine generators, only four are currently in use, for a total power of $6,6\,MVA$. Total energy produced in 2017 was $21,08\,GWh$, which corresponds with a consumption of $5.948.779\,l$ of Diesel, and $18.116\,l$ of motor oil. In Tab.4.1 the main operating data are shown.

Table 4.1: Details on Diesel power plant

Month	**Production [kWh]**	**Peak Power [kW]**	**Diesel cons. [l]**	**Motor oil cons. [l]**
Jan	1.042.635	2.909	314.290	1.983
Feb	1.004.674	2.433	302.790	1.672
Mar	877.302	3.314	259.260	1.936
Apr	1.560.065	4.517	434.500	1.016
May	2.135.728	4.760	597.095	1.392
June	2.074.514	4.811	589.655	2.212
July	1.963.114	4.488	553.220	588
Aug	2.084.646	4.740	581.605	2.045
Sept	1.996.753	4.737	554.250	934
Oct	2.064.933	4.644	565.229	710
Nov	2.088.450	4.747	581.490	2.018
Dec	2.187.553	4.853	615.395	1.610
TOTAL	**21.080.367**	**-**	**5.948.779**	**18.116**

The gensets are operated solely with the droop technique; therefore, they can only provide primary regulation. At the present moment, there is a lack of automated secondary regulation and the frequency is regulated periodically by an operator.
In our PowerFactory model, the array of gensets is represented by a single synchronous machine with equivalent power. When active, this equivalent machine is the reference (slack) bus of the system.

4.2.2 Load

The load is distributed throughout the island and adds up to a maximum power of $4,2\,MW$. As we can see from Fig.4.2, the load profile is similar to a common residential load, with peak request during evening hours, even though there are some factories in the island.

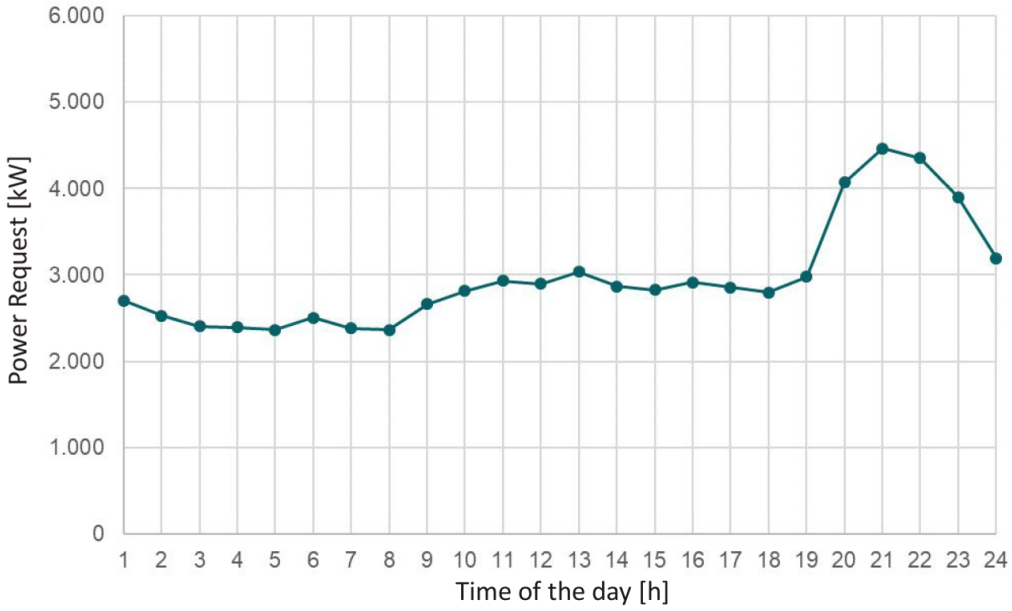

Figure 4.2: Typical day load

Since the only information available for individual loads is the apparent power rating of the MV/LV transformers, we consider this as the maximum power request and assume $cos\varphi = 0.9$ for all of them. This is considered a realistic assumption, as the load is mainly composed of households. Moreover, since the exact location of many loads is unknown, we extimated it based on maps.

4.2.3 Electrical Lines

At the present moment, the grid of Anjouan features a single bus and a radial structure, with feeders represented by 20 kV overhead lines in single circuit configuration. In Fig.4.3 we can see the outline of the island electrical lines. Starting from the main bus in Trenani we can follow two main lines: one (Depart II in Fig.4.5) that goes towards the chief city Mutsamoudou and then covers the northwestern part of the island, and the other one (Depart I) that covers the southeastern part. Along most of the lines runs optical fiber that can be exploited for control purposes, after an agreement with the local internet service provider.

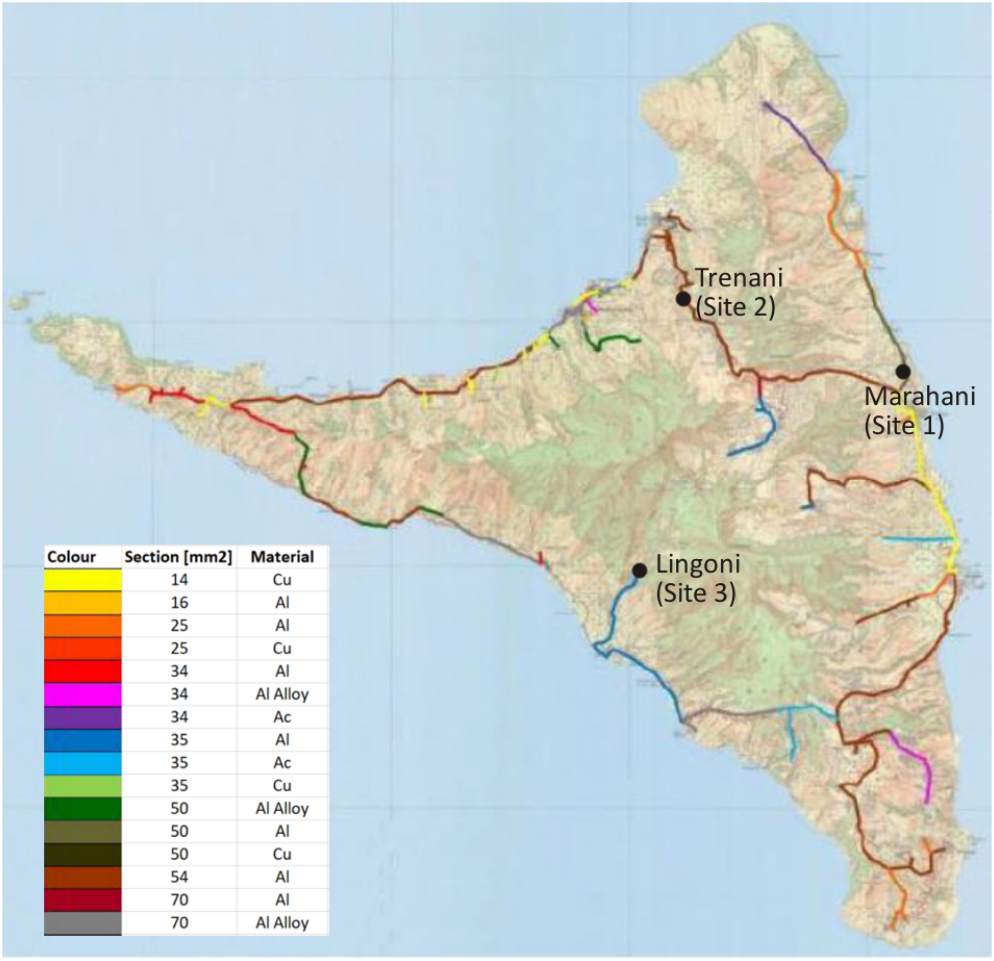

Figure 4.3: Island Map

Given the small length of the lines (visible in Fig.4.5), we represented them in PowerFactory using the lumped parameters model. To do this, we extracted data on electrical per unit length parameters (resistance and inductance) from commercial datasheet, based on the size and material information reported in the legend of Fig.4.3.

4.2.4 Present Load Flow Scenario

In Fig.4.4, we can see the resulting PowerFactory grid in a load flow simulation. The maximum voltage drop is 7% at the end of Depart I and we computed the grid efficiency, which is 96.8%. While these values are in an acceptable range, it is evident that this configuration of the system is highly susceptible to faults. As a matter of fact, a failure at the start of Depart I could cause a blackout in more than half of the island. The addition of PV-BESS plants will enhance the flexibility of the grid and reduce the effects of line faults.

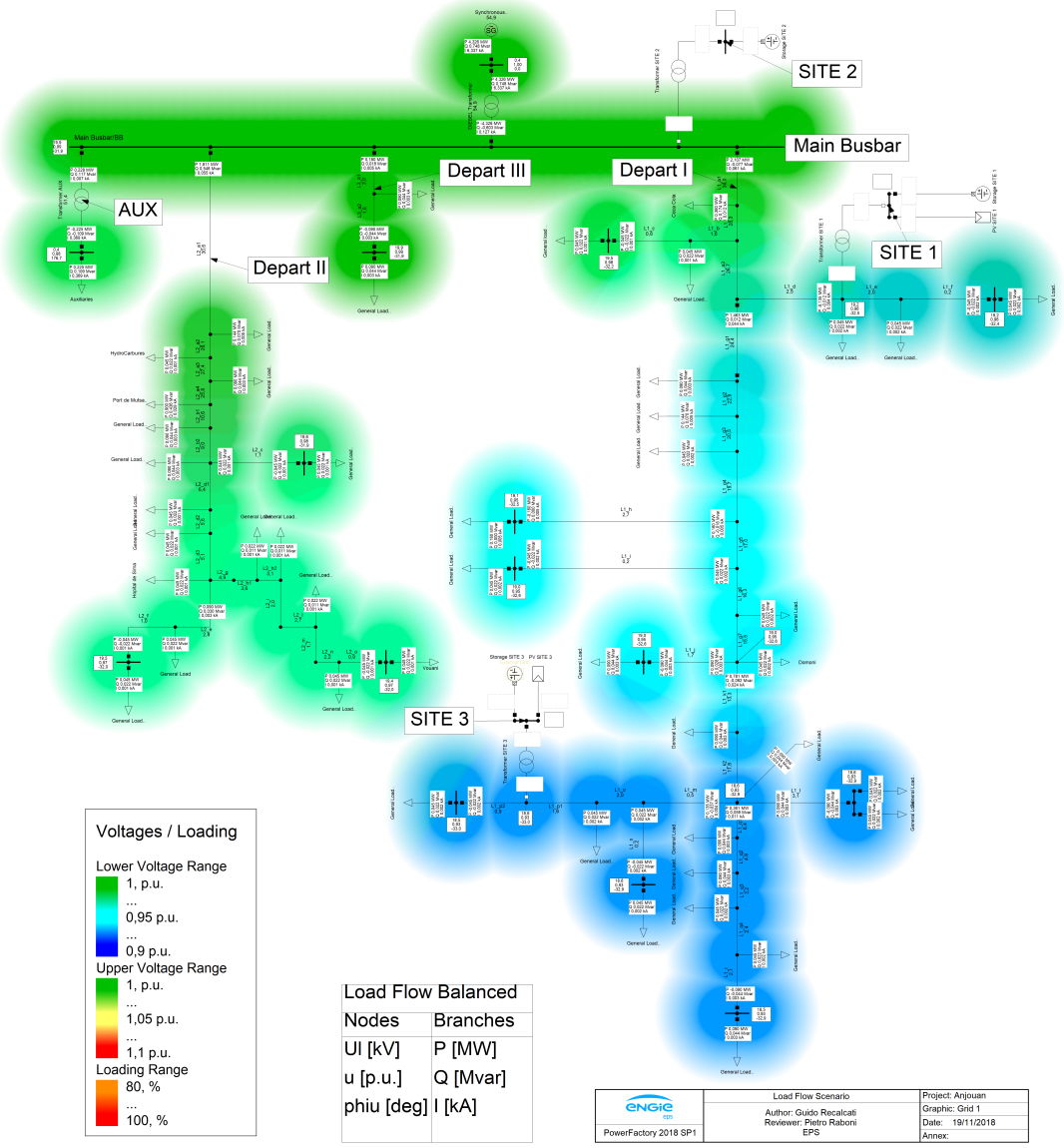

Figure 4.4: Present situation- Load Flow

4.3 Engie-EPS Plan

EPS will realize three new power plants, marked in Fig.4.3:

- Marahani (Site 1) - PV plant for a total power of $2,7\,MVA$, coupled with a Battery Energy Storage System (BESS) with total power of $2,7\,MVA$ and total capacity of $2,9\,MWh$
- Trenani (Site 2) - in correspondence with the existing diesel power plant, Engie-EPS will install a BESS characterized by total power of $2,7\,MVA$ and total capacity of $2,9\,MWh$

- Lingoni (Site3) - PV plant for a total power of $2,7\,MVA$, coupled with a Battery Energy Storage System (BESS) with total power of $2,7\,MVA$ and total capacity of $2,9\,MWh$

In Fig. 4.5 we can observe the layout of the electrical system in the Single Line Diagram (SLD) of the grid.

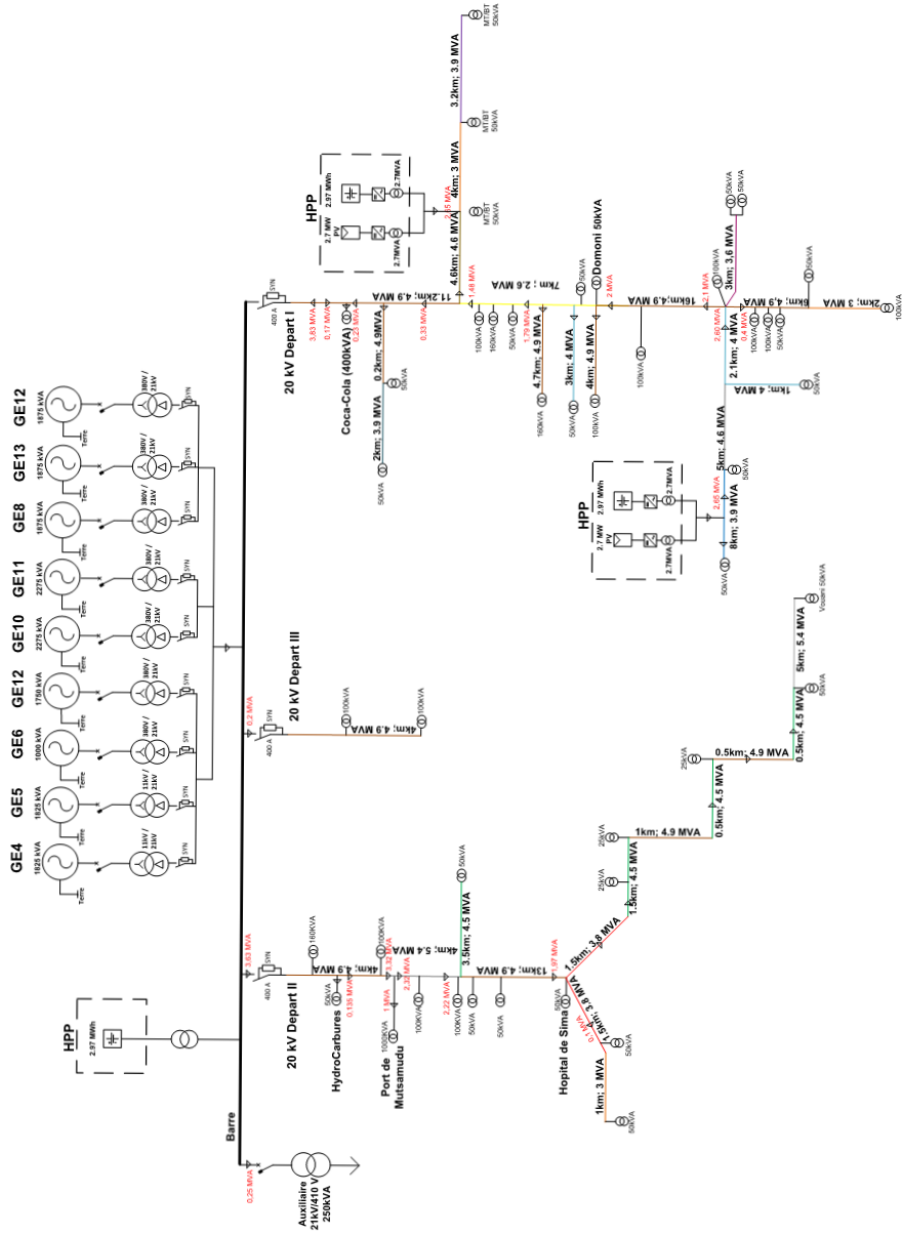

Figure 4.5: Single Line Diagram

4.3.1 Contemporary use of HPP and Gensets

In Fig.4.6 we reported the case of contemporary use of both PV-BESS plants and diesel plants. As we can see, the maximum voltage drop (3%) is at the end of Depart II, while the area around Site 3 has a slight overvoltage (+3%). The efficiency is 98.2%. It is interesting to notice that we have power going from Depart I to the main bus and to the other departures, therefore Engie-EPS will need to change protections to allow this power reverse.

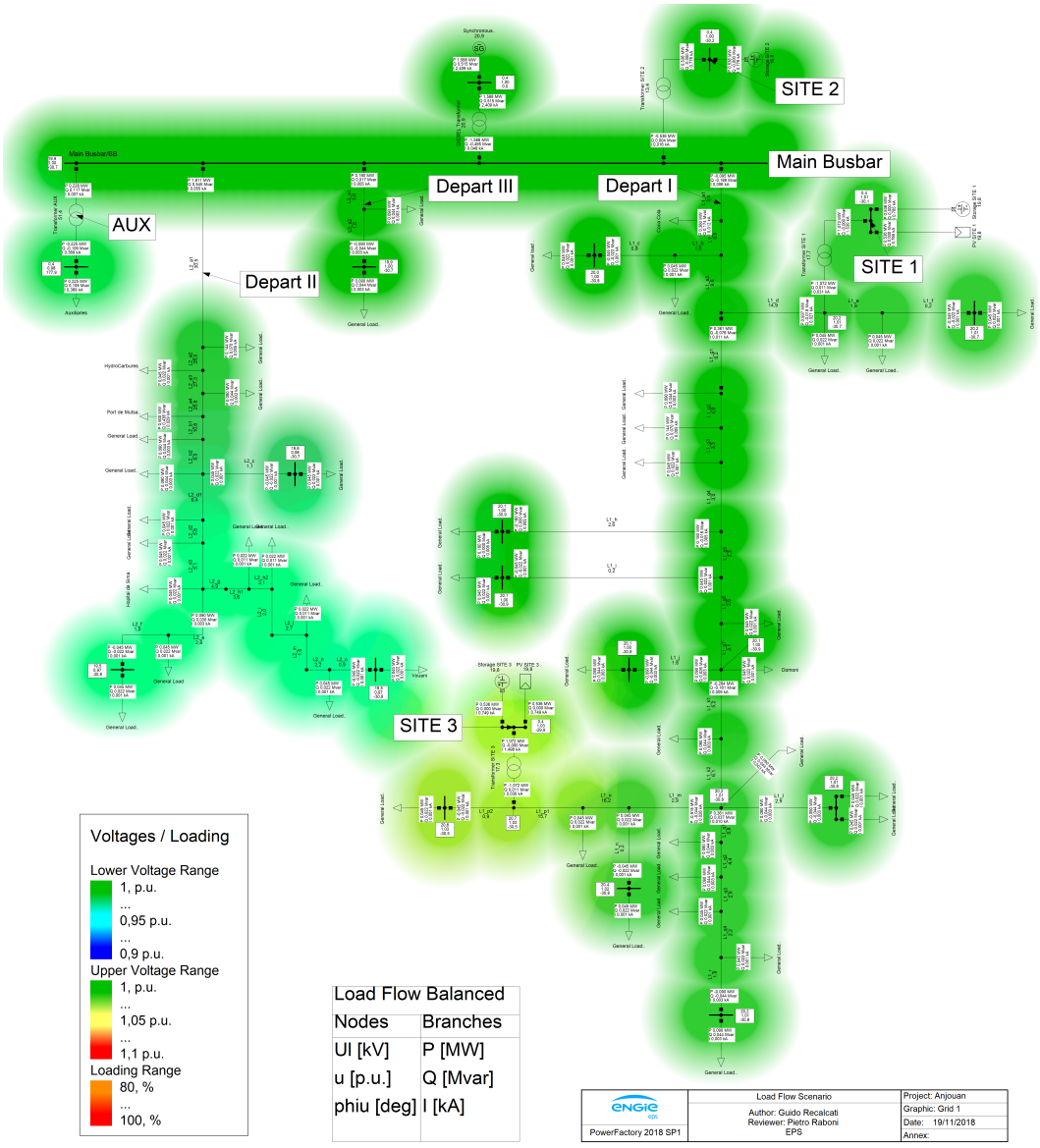

Figure 4.6: HPP and Gensets- Load Flow

4.3.2 Technical challenges

The presence of three distinct generating points across the island implies a three bus grid topology. As a consequence the control system is no more represented by a single Hybrid Power Plant insisting over a single busbar, as in previous Engie-EPS microgrid installations. This implies the use of a larger and more spread out communication network necessary to provide primary and secondary regulation when the generators are distant from each others, which will significantly raise the complexity of the system. Moreover, relying on a public structure (owner of the optical fiber lines) for the communication system presents risks, as high traffic along the lines could cause delays or losses of information. A centralized system in this context would not be robust enough. Therefore, we needed to develop and design a distributed control system that could withstand the possible faults. The results reported in Chapter 3 showed how the controller we designed in Chapter 2 is a valid solution.

4.3.3 Objectives and advantages

The introduction of the storage system and PV plants will significantly reduce fuel consumption: in a first phase, the diesel generators are expected to reduce their energy production to 53.5%; in a second phase, more distant in the future, the objective is to completely switch off the Gensets and only use solar energy from the PVs. This of course will bring both economical and environmental advantages for the island. Moreover, the introduction of our automated primary and secondary frequency controller will generate a significant improvement in power quality.

Chapter 5

Simulations with DIgSILENT PowerFactory

In this chapter, we show the dynamic model of the controller we built in DIgSILENT PowerFactory and we report the result of the RMS simulations we performed, focusing on the behavior of system frequency and generator power output.

5.1 Differences from Simulink model

In the Simulink model we described in Chapters 2 and 3, the generator receives an input power and supplies the load with it. In other words, the inverter is modeled as a power actuator. Now, since we are able to realize the actual electric model of the grid, we model the inverter as an AC voltage source that receives a reference of voltage amplitude and frequency (V_{ref} and f_{ref}), and outputs a sine wave to the grid. It forms the voltage of the grid. This approach is one of the three main inverter control modes and it is usually called grid-forming mode [21] [22]. In this chapter, as in all of this thesis, we focus on the frequency control, so we neglect any complex voltage regulation scheme and we operate the generators as equivalent PV nodes.

Our controller, therefore, will be a little different from the one we have explained in Chapter 3 in the primary control loop. In particular, if we look at the droop equation (with $P_i^* = 0$) :

$$\omega_i = \omega_i^* - m_i \cdot (P_i - P_i^*) = \omega_i^* - m_i \cdot P_i \tag{5.1}$$

In Simulink, we needed P as the controller output and so we solved the equation for it (Fig.5.1a). In PowerFactory, as we mentioned, we need the frequency as the controller output (and inverter input), so we solve the equation for ω_i(Fig.5.1b). The secondary control part of the system, which outputs ω_i^*, does not change.

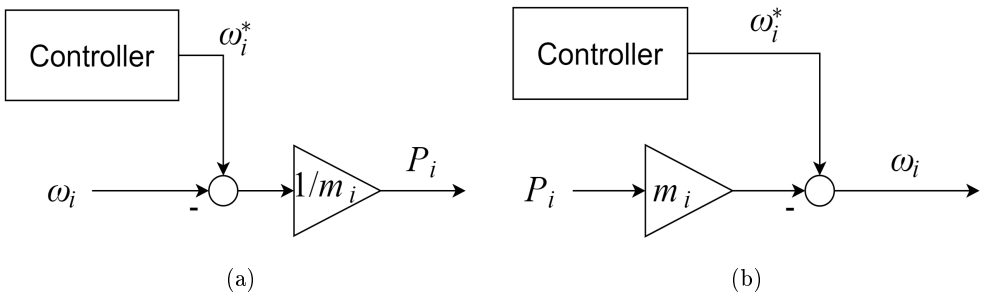

Figure 5.1: Inverter operating modes, droop

5.2 Components of dynamic control system

5.2.1 Composite Frame

In PowerFactory, dynamic modeling has a layer structure. The outermost layer is the composite frame. It is an overview diagram that shows the connections and signal exchanges between slots, and the type of object (element of the system) that has to be assigned to each slot. In Fig. 5.2 we report the frame of our controller (there will be one of these for each generator). As we can see there are three StaPqmea slots, to which we assign three different power meters (one for each power plant in the system). The power signals are then supplied to the power controller slot (ElmF_c) which contains the block definition of the controller we designed. The output from P/f controller and V controller (which is constant as we explained previously) are then connected to the slot of the static generator, which corresponds to the inverter in the grid model (ElmVac).

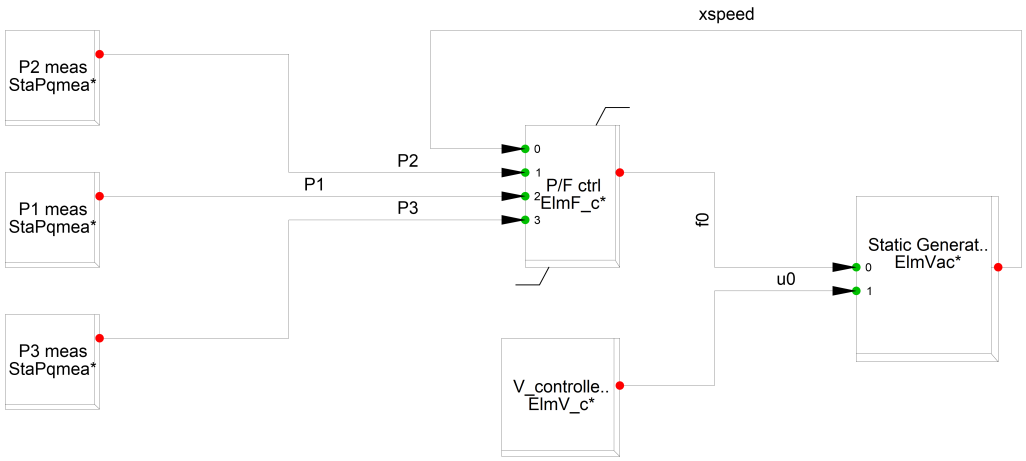

Figure 5.2: Composite frame

5.2.2 Composite block definitions

Block definitions show the mathematical relations between signals using Laplace transform, and they can be assigned to slots. We defined the block to be inserted in the P/f controller slot based on the Simulink block scheme of Chapter 2, with the differences explained previously in this chapter. In Fig.5.3 we can clearly see the difference in the primary regulation section. It is also important to notice the presence of gains a_{12},a_{13} and g_1 which will be used to simulate the various states of the communication network.

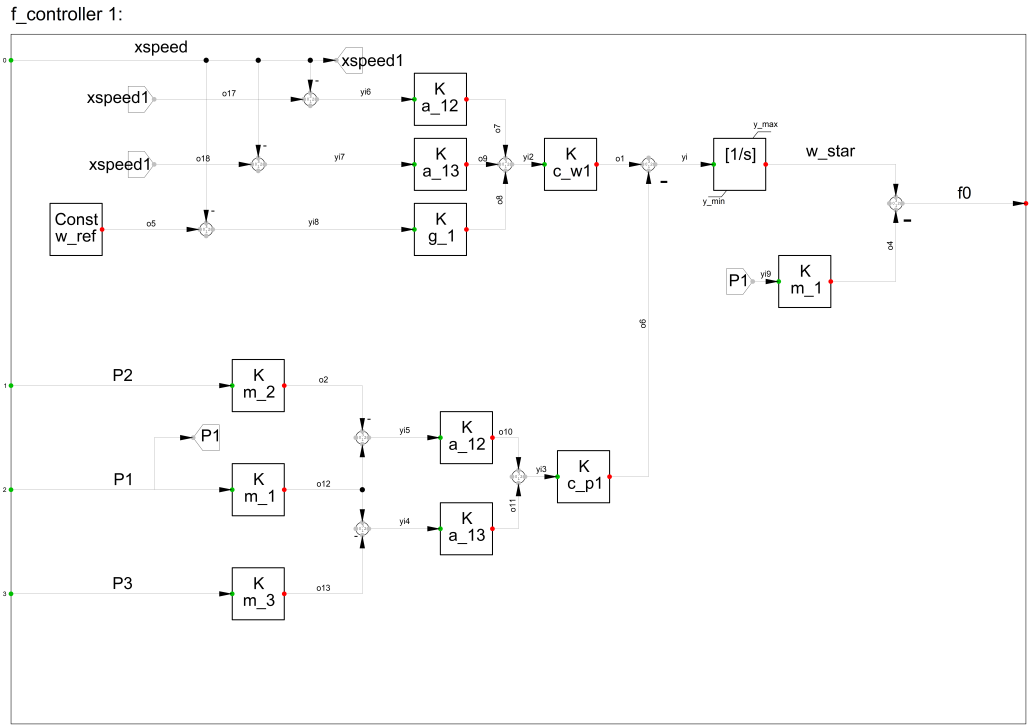

Figure 5.3: Composite frame

5.3 Transient Simulation setup

We will now show the results of the RMS simulations we performed in PowerFactory, where we applied the controller to the BESS inverters, as they are the ones that operate the secondary regulation. The PV plants, instead, are set to give constant power equal to the one we obtained from power flow simulations (0.882 MW per plant).

In order to test our system secondary control performances, we have to introduce a perturbation in power request. In Powerfactory we decided to do this by setting a switch event that opens the switch at the beginning of Depart II after 15 s. This corresponds to a load step of -1.785 MW (-0.42 p.u.), as the load passes from 4.185

MW to 2.4 MW. Even though this is a very large variation, this is considered a realistic scenario, as a fault at the beginning of that line could effectively occur and possibly generate a blackout in that area of the island.
In Table 5.1 we report the set of parameters used in all of the simulations.

Parameter	**Value**	**Parameter**	**Value**
c_w1	1	**m_3**	2%
c_w2	1	**k_11**	0.1
c_w3	1	**k_12**	1
c_p1	1	**k_21**	0.1
c_p2	1	**k_22**	1
c_p3	1	**k_31**	0.1
m_1	2%	**k_32**	1
m_2	2%	**w_ref**	1

Table 5.1: Set of parameters used

As we did in Chapter 3, we will analyze different scenarios changing the parameters regarding the communication system (a_i, g_i). In particular, by assigning null value to any of these parameters, we simulate the failure of a specific communication link, so that we can test the robustness of our system to communication losses.
Hereafter we report some of the most interesting cases, using the numeration we introduced in Chapter 3.

5.4 Normal operating scenario (case 1)

In this scenario there are no faults in the communication system and the controller works as expected. In Fig.5.4 we see the behavior of the system frequency: after the switch event we have an increase of the frequency (xspeed up to 1.005 p.u., 50.25 Hz), but the controller is able to regulate it and bring it back to the nominal value. Therefore our system, as expected, performs the secondary regulation. By looking at the p.u. power outputs of the BESS generators (lower part of Fig.5.4) we can also observe that the controller performs primary regulation, as the total output power (0.093 p.u. or 0.25 MW for each BESS and 0.882 MW from each PV, for a total power of 2.51 MW), matches the power request, taking into account power losses.

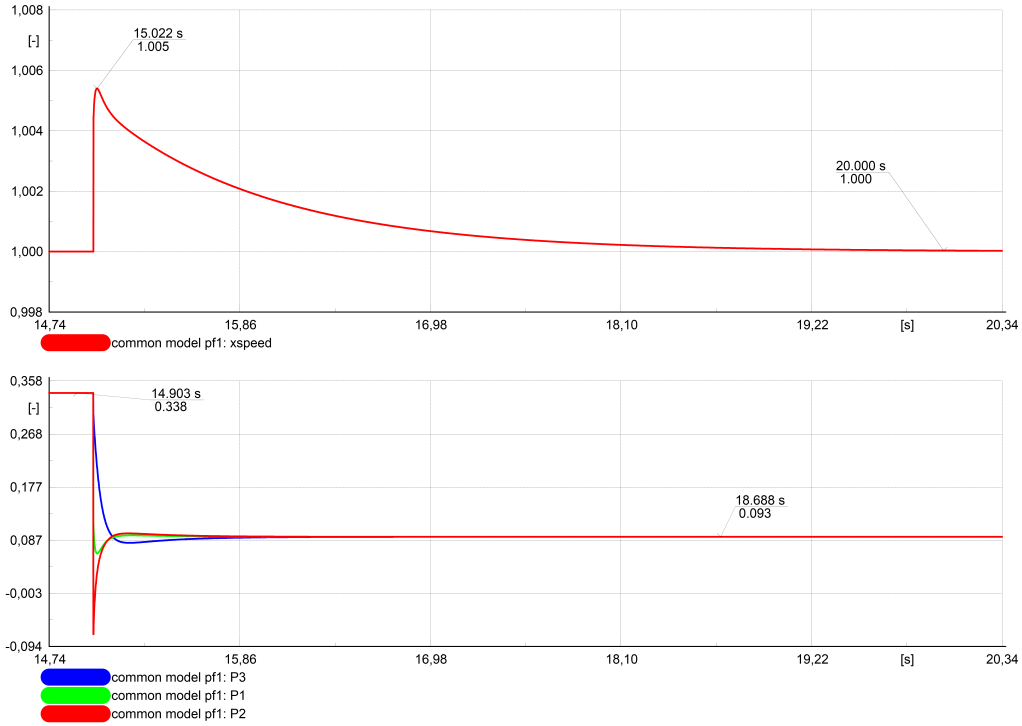

Figure 5.4: p.u. frequency and power, normal scenario

5.5 Case 9

In this scenario, we simulate the failure of the communication link between Site 1 and Site 2 ($a_{12} = 0$). As we can see in Fig.5.5, there is no significant difference from the normal operating scenario. The system performs primary and secondary regulations correctly.

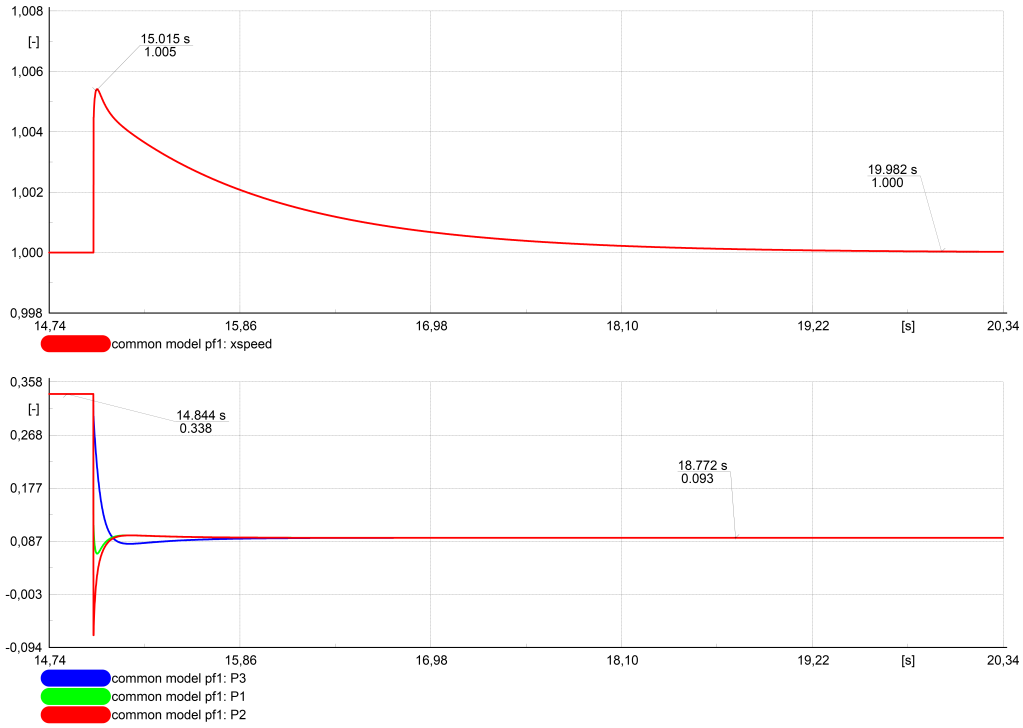

Figure 5.5: p.u. frequency and power, case 9

5.6 Case 2

In this scenario, we simulate the absence of direct reference for the BESS of Site 1 ($g_1 = 0$). In Fig.5.6 we can see that initial and final values of both p.u. power and frequency are the same of the ones of the normal operating scenario, but the behavior of generator 1 (in green) during transient is slightly different, due to the absence of direct reference. The system, however, operates correctly both primary and secondary regulations, and the load is correctly shared between the three BESS, as their final p.u. power is the same (0.093).

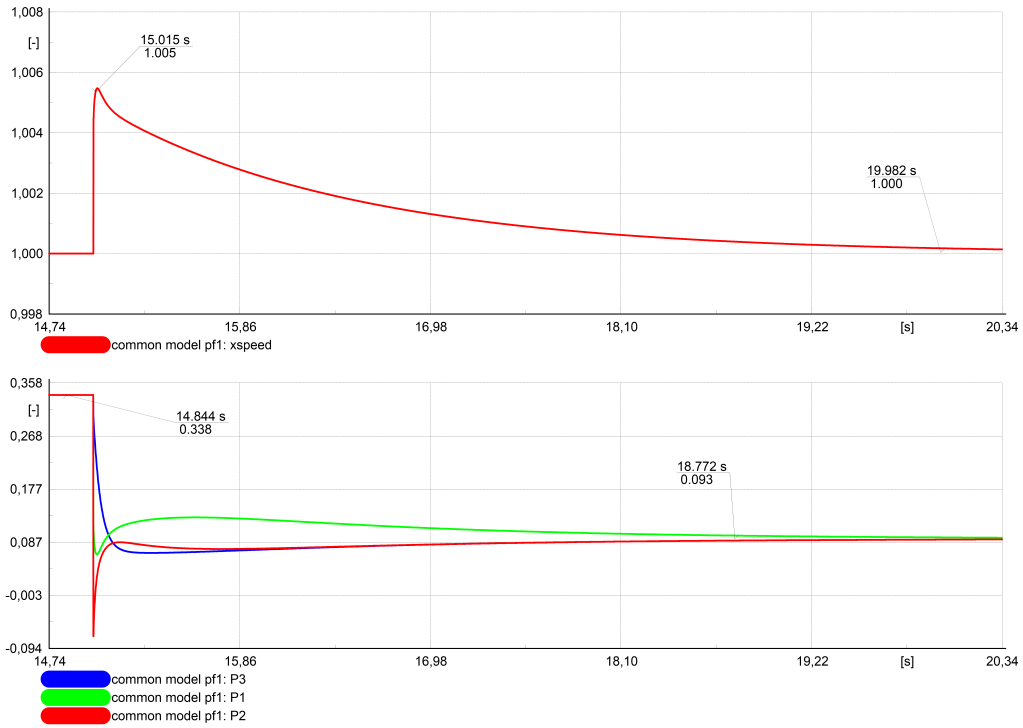

Figure 5.6: p.u. frequency and power, case 2

5.7 Case 8

This scenario simulates the failure of all the communication links between the Leader and the DGs, therefore $g_1 = g_2 = g_3 = 0$. As there is a lack of reference, the system does not operate the secondary regulation, and therefore the frequency does not converge to its nominal value, even if the power request is correctly balanced. In Fig.5.7, as a matter of fact, we can see that the initial and final values of power output correspond to the ones we obtained in the normal operating scenario. By using the droop equation we can use these power values to calculate the frequency of the system before the switch event ($\omega_i = 1 - m_i P_i = 0.993$ p.u.) and after the switch event ($\omega_i = 1 - m_i P_i = 0.998$ p.u.) , which confirms the results of the simulations.

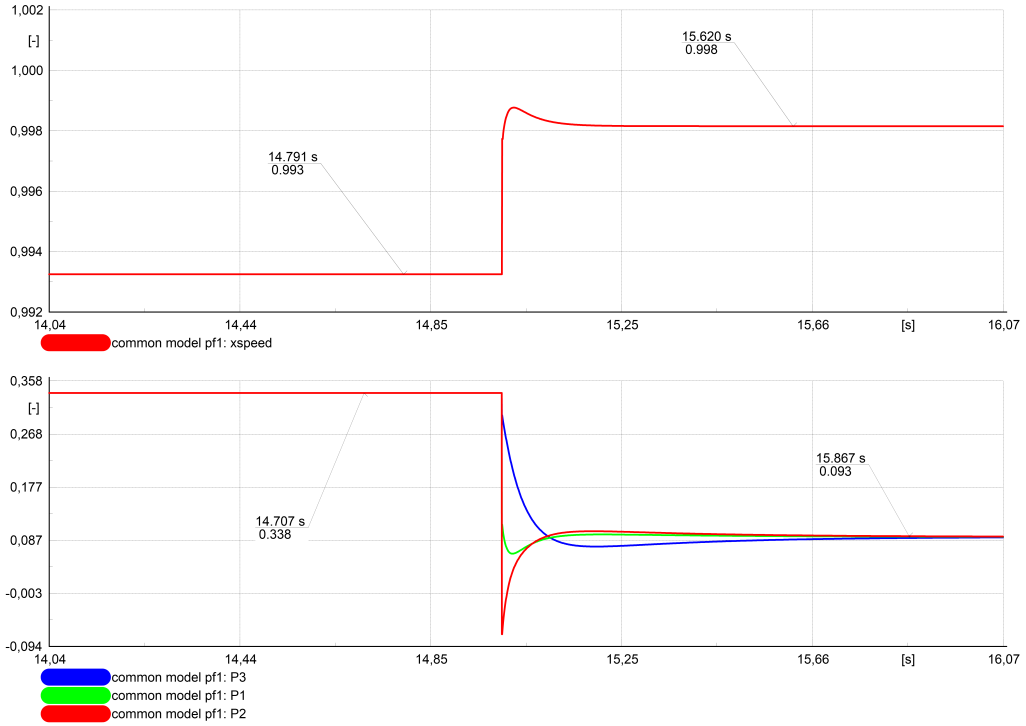

Figure 5.7: p.u. frequency and power, case 8

5.8 Case 26

In this case, Site 1 is isolated from the rest of the communication system ($g_1 = 0$ and $a_{12} = a_{13} = 0$). As a consequence, the inverter of the BESS of Site 1 operates on the droop characteristic without any correction term. In Fig.5.8 we can see that, since we set $P_i^* = 0$ for every DG, BESS number 1 does not give power, and so the other machines operate the regulations. Final power output for them is 0.142 p.u. or 0.385 MW, which together with the power coming from PVs matches correctly the request.

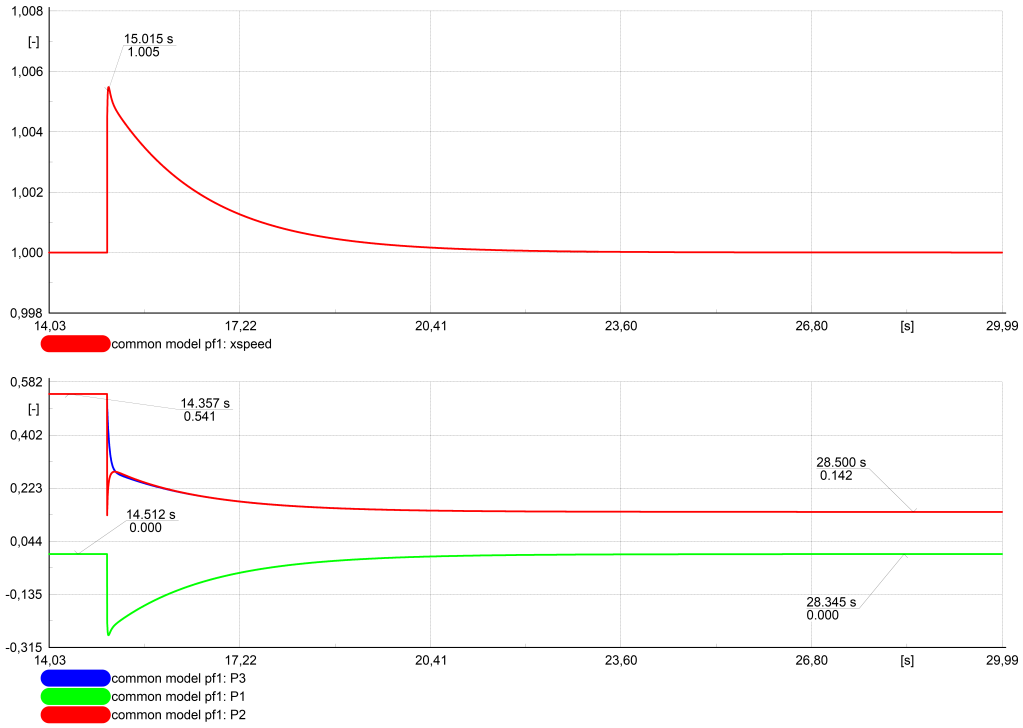

Figure 5.8: p.u. frequency and power, case 26

5.9 Case 12

This case features a spanning tree in the communication graph, and one single connection between leader and Site 3. As we proved in Chapter 2, this is the minimum number of connection which allows the controller to perform correctly. In Fig.5.9 we can observe how the system behaves correctly, but with a longer transient (around 15 s while in case 1 it lasted around 6 s).

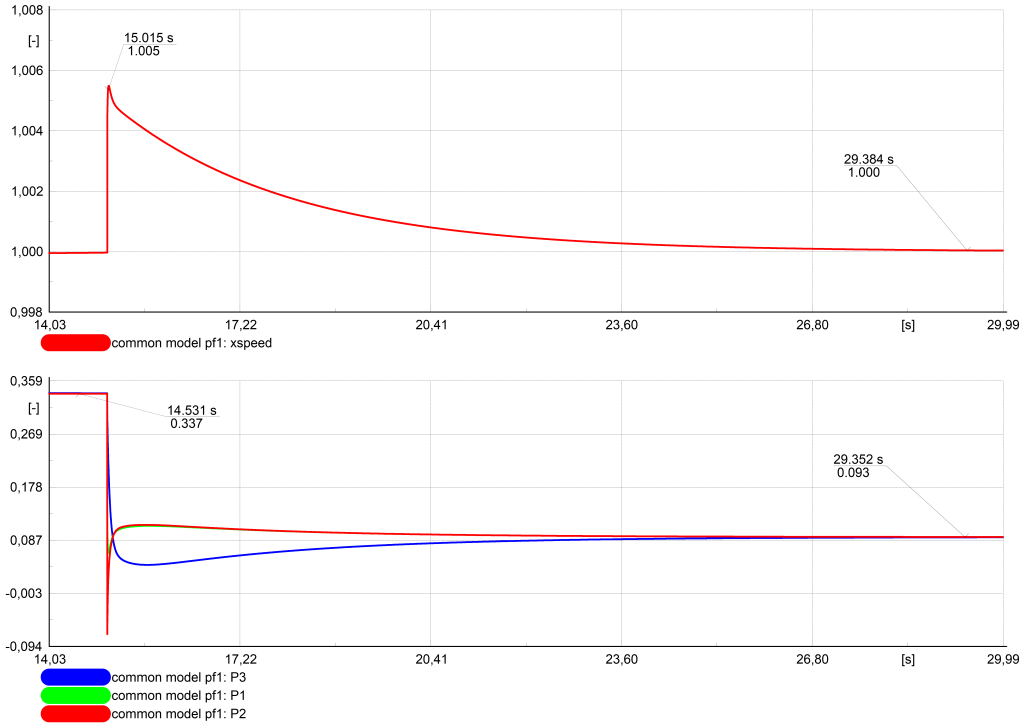

Figure 5.9: p.u. frequency and power, case 12

5.10 Night-time, normal operating scenario

This scenario simulates the same switch event, during night time. The PV power, therefore, is set to 0, and all the island is supplied by the BESS. In this scenario there are no faults in the communication system and the controller works as expected. In Fig.5.10 we see the behavior of the system frequency: after the switch event we have an increase of the frequency (xspeed up to 1.006 p.u.), but the controller is able to regulate it and bring it back to the nominal value. Therefore our system, as expected, performs the secondary regulation. By looking at the p.u. power outputs of the generators we can also observe that the controller performs primary regulation, as the total output power (2,514 MW), matches the power request, taking into account power losses.

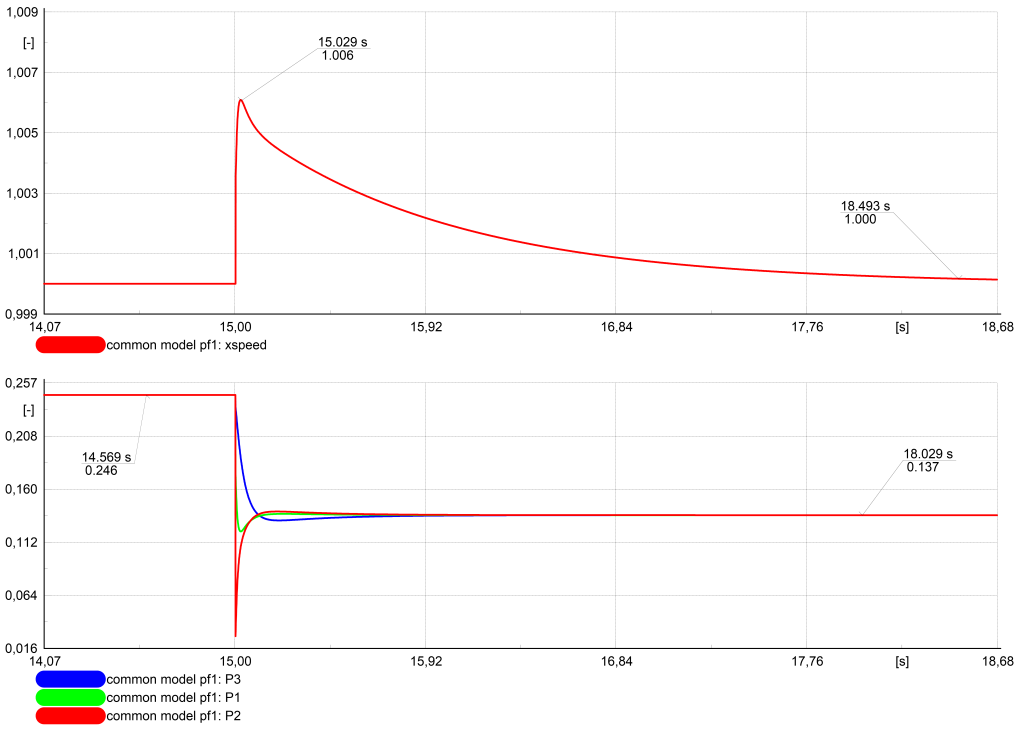

Figure 5.10: pu frequency and power, night-time normal scenario

5.11 Model validation

To show that the Simulink model is equivalent to the PowerFactory one, we tested the former under the same conditions as the latter. As a first step we gave as input the load variation shown in Fig. 5.11

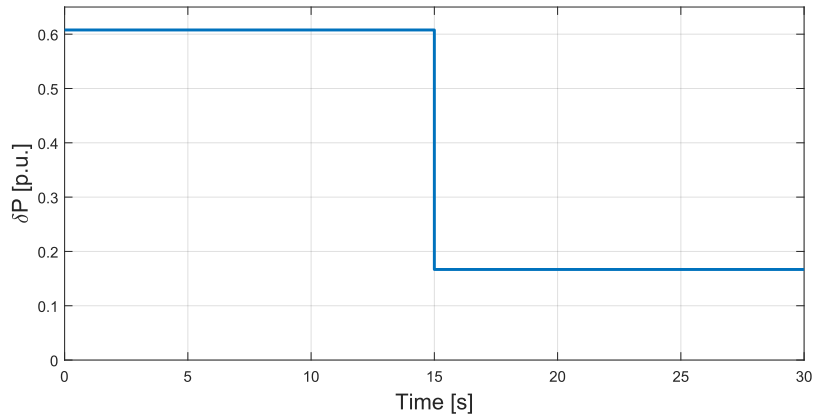

Figure 5.11: Input Step

This profile is relative to a total load of 4.5 MW which includes power losses. The initial and final values (respectively 0.61 p.u. and 0.17 p.u.) are computed excluding the power supplied by PV plants (2x0.882 MW each, or 2x20% of the total load). Considering that in Simulink, the controller parameters are relative to the total load (4.5 MW), while in PowerFactory they are based on the inverter rating (2.7 MW), we need to operate a base change on these parameters, in particular on the droop coefficients. We can do this as shown in eq.5.2, while in Table 5.2 we can see the complete set of parameters used:

$$m_{pu,Load} = m_{pu,Machine} \cdot \frac{P_{base,Load}}{P_{base,Machine}} = 0.02 \cdot \frac{4.5\,MW}{2.7\,MW} = 3.1\% \tag{5.2}$$

Table 5.2: Set of parameters used

Parameter	**Value**	**Parameter**	**Value**
c_w1	1	**k_11**	0.1
c_w2	1	**k_12**	1
c_w3	1	**k_21**	0.1
c_p1	1	**k_22**	1
c_p2	1	**k_31**	0.1
c_p3	1	**k_32**	1
m_1	3.1%	**T_a**	5
m_2	3.1%	**D**	0
m_3	3.1%	**w_ref**	0

It is important to notice that we set D = 0 and load transfer function $F_{load}(s) = \frac{1}{T_a s}$, so that load power is not sensible to frequency variation. This reflects the way loads are set in PowerFactory. We ran simulations with absence of communication between leader node and distributed generators (case 8), and in normal operating scenario (case 1). Main results are reported in Fig.5.12 and Fig.5.13.

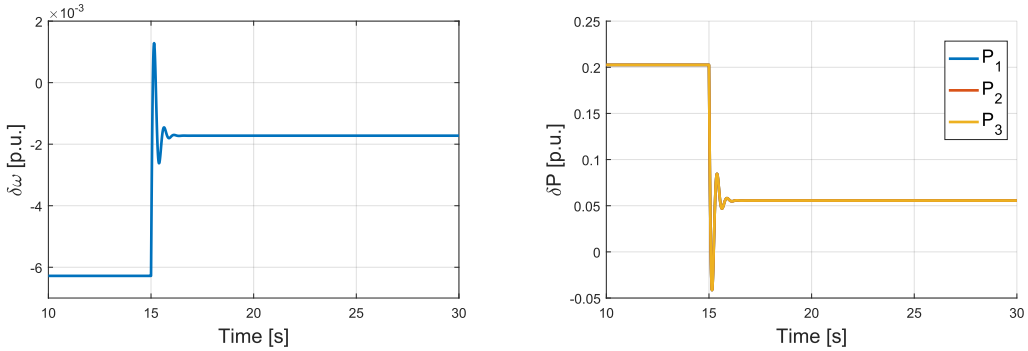

(a) Frequency variation case 8 (b) Machine loading case 8

Figure 5.12: Case 8 results

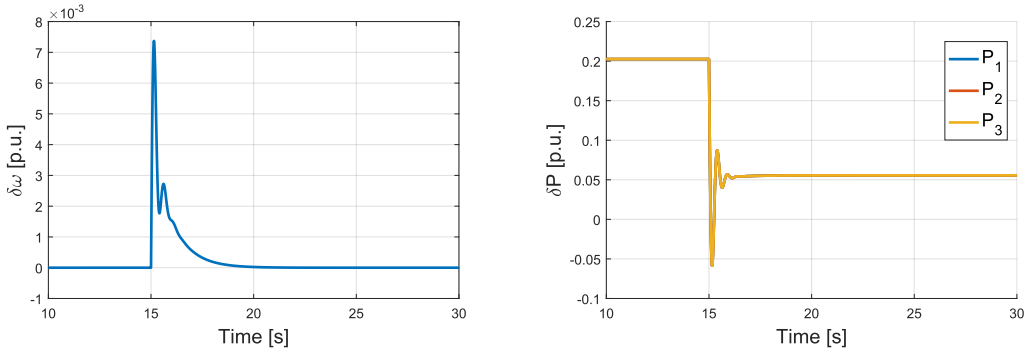

(a) Frequency variation case 1 (b) Machine loading case 8

Figure 5.13: Case 1 results

In particular, in Fig.5.12b and in Fig.5.13b we can see that, in both cases, the machine loading corresponds to the one we obtained in Powerfactory, both before (33%) and after (9%) the load change. In Fig.5.12a, moreover, we can observe that the frequency variation values in case 8 (6.2%¸ before the load change, and 1.7%¸ after the load change), reflect the ones obtained in PowerFactory (respectively 0.993 p.u. and 0.998 p.u.).

So, by confronting these results we can conclude that the two systems have the same overall behavior, as the initial and final values coincide. The behavior during transient, however, is slightly different. These differences may be due to the some hidden

PowerFactory dynamic behaviors, for example in the modeling of the measuring elements (StaPqmea) or in the model of the inverters (ElmVac).

5.12 Conclusions

From the simulations of this chapter we can see that the system is able to operate correctly in a grid environment, and it is robust to communication failures. The results are in line with the ones we obtained in Simulink. In particular case 12 shows how, even with minimal working conditions, the controller corrects the frequency in an acceptable time.

Conclusions

This thesis aimed at developing a secondary frequency controller for the isolated Microgrid of the island of Anjouan, Comores. The typical control challenges of Microgrids, as well as the peculiar constraints of the island (in particular the multi-bus topology and the insufficient reliability of the communication infrastructures), implied that the use of a traditional centralized controller was not suitable for this application, because too sensitive to loss of communications. In order to realize a controller more robust against communication failures, we opted for a solution which literature refers to as distributed. This kind of controller does not rely solely on communication between a central unit and distributed generators, but also exploits a secondary communication network which allows the exchange of frequency and power data between neighboring generators, building the so called *local neighborhood tracking error* for each generator.
After an analytical study of the proposed controller, exploiting Lyapunov and graph theories, we built a Simulink model of a three-generators system based on the proposed controller. On this model we have run various simulation, applying a load power step in different communication scenarios. The system proved to be robust against communication failures by correctly performing both primary and secondary regulations. The minimal working configuration consisted of a spanning-tree graph with a single connection to the leader.
By realizing a DIgSILENT PowerFactory model of the grid of Anjouan, we were able to test the proposed controller on a real potential application case. Again, simulating different communication failures and imposing a load decrease, proved how the system is able to correctly perform both primary and secondary regulation, just as it did in Simulink, considering also power losses.
Possible future development of this thesis might deal with:

- the distributed voltage regulation, applying the same constraints and conditions
- integration with Engie-EPS Energy Management System
- stability study and assessment effect of communication latencies and system parameters over poles position

Bibliography

[1] Cherry Yuen, Alexandre Oudalov, and Adrian Timbus. The provision of frequency control reserves from multiple microgrids. *IEEE Transactions on Industrial Electronics*, 58(1):173–183, Jan 2011.

[2] Ali Ipakchi and Farrokh Albuyeh. Grid of the future. *IEEE Power and Energy Magazine*, 7(2):52–62, Mar 2009.

[3] R.H. Lasseter. MicroGrids. In *2002 IEEE Power Engineering Society Winter Meeting. Conference Proceedings (Cat. No.02CH37309)*. IEEE.

[4] U.S. Department of Energy. Doe microgrid workshop report. Technical report, 2011.

[5] Hatziargyriou et al. Microgrids-large scale integration of microgeneration to low voltage grids. *Proceedings of CIGRE 2006*, 2006.

[6] IEEE PES Task Force on Microgrid Stability Analysis and Modeling. Microgrid stability definitions, analysis, and modeling. Technical report, IEEE Power & Energy Society, 2018.

[7] R. Marin and M. Valtorta. *Trasmissione ed interconnessione*. CEDAM, 1973.

[8] R. Marconato. *Electric power systems*. Number Vol. 2. CEI, 2004.

[9] Josep M. Guerrero, Mukul Chandorkar, Tzung-Lin Lee, and Poh Chiang Loh. Advanced control architectures for intelligent microgrids—part i: Decentralized and hierarchical control. *IEEE Transactions on Industrial Electronics*, 60(4):1254–1262, Apr 2013.

[10] Prabha Kundur. *Power System Stability And Control*. McGraw-Hill, 1994.

[11] H. Bevrani. *Robust Power System Frequency Control*. Power Electronics and Power Systems. Springer International Publishing, 2014.

[12] ENTSO-E. *Continental Europe Operation Handbook. Load-Frequency Control and Performance*, Apr 2009.

[13] Xiaoqing Lu, Xinghuo Yu, Jingang Lai, Yaonan Wang, and Josep M. Guerrero. A novel distributed secondary coordination control approach for islanded microgrids. *IEEE Transactions on Smart Grid*, 9(4):2726–2740, July 2018.

[14] Xiangyu Wu and Chen Shen. Distributed optimal control for stability enhancement of microgrids with multiple distributed generators. *IEEE Transactions on Power Systems*, 32(5):4045–4059, Sept 2017.

[15] Xiaoqing Lu, Renquan Lu, Shihua Chen, and Jinhu Lu. Finite-time distributed tracking control for multi-agent systems with a virtual leader. *IEEE Transactions on Circuits and Systems I*, 60(2):352–362, Feb 2013.

[16] L. Magni and R. Scattolini. *Complementi di controlli automatici*. Pitagora, 2006.

[17] Jean-Jacques E Slotine and Weiping Li. *Applied nonlinear control*. Pearson, 1991.

[18] Ali Bidram, Frank L. Lewis, Zhihua Qu, and Ali Davoudi. Secondary control of microgrids based on distributed cooperative control of multi-agent systems. *IET Generation, Transmission & Distribution*, 7(8):822–831, Aug 2013.

[19] Hongwei Zhang, F. L. Lewis, and A. Das. Optimal design for synchronization of cooperative systems: State feedback, observer and output feedback. *IEEE Transactions on Automatic Control*, 56(8):1948–1952, Aug 2011.

[20] Zhihua Qu, Jing Wang, and Richard A. Hull. Cooperative control of dynamical systems with application to autonomous vehicles. *IEEE Transactions on Automatic Control*, 53(4):894–911, May 2008.

[21] Joan Rocabert, Alvaro Luna, Frede Blaabjerg, and Pedro Rodríguez. Control of power converters in AC microgrids. *IEEE Transactions on Power Electronics*, 27(11):4734–4749, Nov 2012.

[22] Xiongfei Wang, Josep M. Guerrero, Zhe Chen, and Frede Blaabjerg. Distributed energy resources in grid interactive AC microgrids. In *The 2nd International Symposium on Power Electronics for Distributed Generation Systems*. IEEE, June 2010.

[23] Robert Grone, Charles R. Johnson, Eduardo M. Sa, and Henry Wolkowicz. Normal matrices. *Linear Algebra and its Applications*, 87:213–225, mar 1987.

Appendix A

Details on chapter 2 proofs

A.1 Local neighborhood tracking error

For the $i-th$ bus, we can write the expression of the local neighborhood tracking error:

$$e_{\omega i} = \sum_{j \in N} a_{ij}(\omega_i - \omega_j) + g_i(\omega_i - \omega_{ref}) \tag{A.1}$$

We will now prove how eq. A.1 is equivalent to:

$$\boldsymbol{e} = (L + G_{lead})(\boldsymbol{\omega} - \boldsymbol{\omega}_{ref}) \equiv (L + G_{lead})\boldsymbol{\delta} \tag{A.2}$$

We start by writing explicitly the $i-th$ row of each one of the matrices used in eq. A.2.

$$A_i = \begin{bmatrix} a_{i1} & a_{i2} & ... & a_{ii} = 0 & ... & a_{iN} \end{bmatrix} \tag{A.3}$$

$$D_i = \begin{bmatrix} 0 & 0 & ... & \sum_{j \in N_i} a_{ij} & ... & 0 \end{bmatrix} \tag{A.4}$$

$$G_{lead,i} = \begin{bmatrix} 0 & 0 & ... & g_i & ... & 0 \end{bmatrix} \tag{A.5}$$

$$L_i = D_i - A_i = \begin{bmatrix} -a_{i1} & -a_{i2} & ... & \sum_{j \in N_i} a_{ij} & ... & -a_{iN} \end{bmatrix} \tag{A.6}$$

$$B_i = L_i + G_{lead,i} = \begin{bmatrix} -a_{i1} & -a_{i2} & ... & \sum_{j \in N_i} a_{ij} + g_i & ... & -a_{iN} \end{bmatrix} \tag{A.7}$$

$$\boldsymbol{\delta} = \begin{bmatrix} v_1 - v_{ref} & v_2 - v_{ref} & ... & v_i - v_{ref} & ... & v_N - v_{ref} \end{bmatrix}^T \tag{A.8}$$

$$
\begin{aligned}
B_i \cdot \boldsymbol{\delta} &= -a_{i1}(v_1 - v_{ref}) + \\
&- a_{i2}(v_2 - v_{ref}) \dots + (\sum_{j \in N_i} a_{ij} + g_i)(v_i - v_{ref}) \dots - a_{iN}(v_N - v_{ref}) = \\
&= -a_{i1}(v_1 - v_{ref}) - a_{i2}(v_2 - v_{ref}) \dots + [g_i(v_i - v_{ref}) + \\
&+ a_{i1}(v_i - v_{ref}) + a_{i2}(v_i - v_{ref}) \dots + a_{iN}(v_i - v_{ref})] \dots + \\
&- a_{iN}(v_N - v_{ref}) = \\
&= g_i(v_i - v_{ref}) + a_{i1}(v_i - v_1) + a_{i2}(v_i - v_2) \dots + a_{iN}(v_i - v_N) = \\
&= \sum_{j \in N_i} a_{ij}(v_i - v_j) + g_i(v_i - v_{ref}) \qquad \square
\end{aligned} \tag{A.9}
$$

A.2 Lemma 1

If $\mathcal{G}$ has a spanning tree, and $g_i \neq 0$ for at least one root node, then:

$$||\delta|| \leq ||\boldsymbol{e}||/\sigma_{min,B} \tag{A.10}$$

Where $\sigma_{min,B}$ is the minimum singular value of $B = (L + G_{lead})$.
We can start by verifying that B^{-1},which, for the sake of convenience, we will call C, is a normal matrix. This means proving that $C^*C = CC^*$ (where C^* it's the conjugate transpose of C) [23]. This is easily done by remembering that B is real and symmetric, and so will be B^{-1}. Thanks to the proprieties of normal matrices we can say that the singular values of B^{-1} are the absolute values of its eigenvalues:

$$\sigma_{i,B^{-1}} = |\lambda_{i,B^{-1}}| \tag{A.11}$$

It is also important to remember that the eigenvalues of B^{-1} are equal to the inverse of the ones of B:

$$|\lambda_{i,B^{-1}}| = \frac{1}{|\lambda_{i,B}|} \tag{A.12}$$

Solving eq.A.2 for $\boldsymbol{\delta}$, we get $\boldsymbol{\delta} = B^{-1}\boldsymbol{e}$.
We will now use the Frobenius norm, which is defined as:

$$||A|| = \sqrt{\sum_{i=1}^{m}\sum_{j=1}^{n}(a_{ij})^2} = \sqrt{\sum_{i=1}^{min(m,n)}[\sigma_{i,A}]^2} \tag{A.13}$$

And since this norm is sub-moltiplicative, which means:

$$||XY|| \leq ||X|| \cdot ||Y|| \, \forall \, X, Y \in K^{NxN} \tag{A.14}$$

We can state that:

$$\begin{aligned} ||B^{-1}\boldsymbol{e}|| &\leq ||B^{-1}|| \cdot ||\boldsymbol{e}|| \\ ||\boldsymbol{\delta}|| &\leq ||B^{-1}|| \cdot ||\boldsymbol{e}|| \\ ||\boldsymbol{\delta}|| &\leq \sqrt{\sum_{i=1}^{N} [\sigma_{i,B^{-1}}]^2} \cdot ||\boldsymbol{e}|| \\ ||\boldsymbol{\delta}|| &\leq \sqrt{\sum_{i=1}^{N} \frac{1}{|\lambda_{i,B}|^2}} \cdot ||\boldsymbol{e}|| \end{aligned} \tag{A.15}$$

Now by maximizing every term of the last summation we can write:

$$\sqrt{\sum_{i=1}^{N} \frac{1}{|\lambda_{i,B}|^2}} \cdot ||\boldsymbol{e}|| \leq \sqrt{N \cdot \frac{1}{|\lambda_{min,B}|^2}} \cdot ||\boldsymbol{e}|| \tag{A.16}$$

Therefore:

$$||\boldsymbol{\delta}|| \leq \frac{\sqrt{N}}{|\lambda_{min,B}|} \cdot ||\boldsymbol{e}|| \tag{A.17}$$

$$||\boldsymbol{\delta}|| \leq \frac{\sqrt{N}}{\sigma_{min,B}} \cdot ||\boldsymbol{e}|| \tag{A.18}$$

A.3 Lemma 2

We define a matrix $P = diag\{1/w_i\}$ where w_i are the elements of a vector $\boldsymbol{w} = B^{-1} \cdot \mathbf{1}_N$, where $B \equiv (L + G)$. We will now prove that $Q \equiv (PB + B^T P)$ is positive definite by proving that it is real and symmetric. To prove that Q is real is pretty straightforward, as all elements of the matrices that are used to build it are real. On the other hand we can prove that Q is symmetric by computing its $i - th$ row as follows:

$$P = diag\{1/w_i\} \qquad B = \begin{bmatrix} b_{11} & b_{12} & ... & b_{1i} & ... & b_{1N} \\ b_{21} & b_{22} & ... & b_{2i} & ... & b_{2N} \\ ... & ... & ... & ... & ... & ... \\ b_{i1} & b_{i2} & ... & b_{ii} & ... & b_{iN} \\ ... & ... & ... & ... & ... & ... \\ b_{N1} & b_{N2} & ... & b_{Ni} & ... & b_{NN} \end{bmatrix} \tag{A.19}$$

$$PB_i = \begin{bmatrix} \frac{b_{i1}}{w_i} & \frac{b_{i2}}{w_i} & \dots & \frac{b_{ii}}{w_i} & \dots & \frac{b_{iN}}{w_i} \end{bmatrix} \tag{A.20}$$

$$B^T P_i = \begin{bmatrix} \frac{b_{1i}}{w_1} & \frac{b_{2i}}{w_2} & \dots & \frac{b_{ii}}{w_i} & \dots & \frac{b_{Ni}}{w_N} \end{bmatrix} \tag{A.21}$$

$$Q_i = PB_i + B^T P_i = \begin{bmatrix} \frac{b_{i1}}{w_i} + \frac{b_{1i}}{w_1} & \frac{b_{i2}}{w_i} + \frac{b_{2i}}{w_2} & \dots & \frac{b_{ii}}{w_i} + \frac{b_{ii}}{w_i} & \dots & \frac{b_{iN}}{w_i} + \frac{b_{Ni}}{w_N} \end{bmatrix} \tag{A.22}$$

From eq.A.22 it is clear how the $i-th$ row is equal to the $i-th$ column transposed, because B is symmetric, as $b_{ij} = -a_{ij} \forall\, i \neq j;\ i,j \in N$, and matrix A is symmetric (so $a_{ij} = a_{ji} \forall\, i \neq j;\ i,j \in N$). This make Q symmetric, and therefore positive definite, for the properties of symmetric and real matrices.

A.4 Theorem 1

Using eq.2.12, we can write the expression of the global input vector:

$$\boldsymbol{u}_\omega = [u_{\omega 1}, u_{\omega 2} ... u_{\omega N}]^T = -c_\omega \boldsymbol{e} \tag{A.23}$$

And remembering that:

$$\boldsymbol{e} = B\boldsymbol{\delta}, \qquad\qquad \dot{\boldsymbol{\delta}} = -c_v \boldsymbol{e} \tag{A.24}$$

We get:

$$\dot{\boldsymbol{e}} = B\dot{\boldsymbol{\delta}} \Rightarrow \dot{\boldsymbol{e}} = -c_v B\boldsymbol{e} \tag{A.25}$$

We define a Lyapunov function candidate:

$$V = \frac{1}{2}\boldsymbol{e}^T P \boldsymbol{e}, \qquad\qquad P = P^T \qquad\qquad P > 0 \tag{A.26}$$

Its derivative is:

$$\dot{V} = \frac{1}{2}[\dot{\boldsymbol{e}}^T P\boldsymbol{e} + \boldsymbol{e}^T P\dot{\boldsymbol{e}}] \tag{A.27}$$

Now considering 2.12 and $\dot{\boldsymbol{\delta}} = \dot{\boldsymbol{\omega}} = -c_\omega \boldsymbol{e}$, we can see that:

$$\dot{V} = \frac{1}{2}[\boldsymbol{e}^T(-c_v B^T)P\boldsymbol{e} + \boldsymbol{e}^T P(-c_v B)\ \boldsymbol{e}] = \tag{A.28}$$

$$= -\frac{1}{2}c_v[\boldsymbol{e}^T B^T P\boldsymbol{e} + \boldsymbol{e}^T PB\ \boldsymbol{e}] = \tag{A.29}$$

$$= -\frac{1}{2}c_v \boldsymbol{e}^T[B^T P + PB]\boldsymbol{e} \tag{A.30}$$

Using what we proved in Lemma 1 and Lemma 2, it is clear how, being $Q = [B^T P + PB]$ definite positive, $\dot{V}$ is definite negative and so for Lyapunov Theorem [16] $\boldsymbol{e}$ is asymptotically stable. Moreover, from Lemma 1, we see that $\boldsymbol{\delta}$ is asymptotically stable, so $\boldsymbol{f}$ synchronizes to $\boldsymbol{f}_{ref}$. This completes the proof.

Appendix B

Operating scenarios table

Case	g1	g2	g3	a12	a13	a23	Case	g1	g2	g3	a12	a13	a23
1	1	1	1	1	1	1	**33**	1	1	1	1	1	0
2	0	1	1	1	1	1	**34**	0	1	1	1	1	0
3	1	0	1	1	1	1	**35**	1	0	1	1	1	0
4	0	0	1	1	1	1	**36**	0	0	1	1	1	0
5	1	1	0	1	1	1	**37**	1	1	0	1	1	0
6	0	1	0	1	1	1	**38**	0	1	0	1	1	0
7	1	0	0	1	1	1	**39**	1	0	0	1	1	0
8	0	0	0	1	1	1	**40**	0	0	0	1	1	0
9	1	1	1	0	1	1	**41**	1	1	1	0	1	0
10	0	1	1	0	1	1	**42**	0	1	1	0	1	0
11	1	0	1	0	1	1	**43**	1	0	1	0	1	0
12	0	0	1	0	1	1	**44**	0	0	1	0	1	0
13	1	1	0	0	1	1	**45**	1	1	0	0	1	0
14	0	1	0	0	1	1	**47**	1	0	0	0	1	0
15	1	0	0	0	1	1	**46**	0	1	0	0	1	0
16	0	0	0	0	1	1	**48**	0	0	0	0	1	0
17	1	1	1	1	0	1	**49**	1	1	1	1	0	0
18	0	1	1	1	0	1	**50**	0	1	1	1	0	0
19	1	0	1	1	0	1	**51**	1	0	1	1	0	0
20	0	0	1	1	0	1	**52**	0	0	1	1	0	0
21	1	1	0	1	0	1	**53**	1	1	0	1	0	0
22	0	1	0	1	0	1	**54**	0	1	0	1	0	0
23	1	0	0	1	0	1	**55**	1	0	0	1	0	0
24	0	0	0	1	0	1	**56**	0	0	0	1	0	0
25	1	1	1	0	0	1	**57**	1	1	1	0	0	0
26	0	1	1	0	0	1	**58**	0	1	1	0	0	0
27	1	0	1	0	0	1	**59**	1	0	1	0	0	0
28	0	0	1	0	0	1	**60**	0	0	1	0	0	0
29	1	1	0	0	0	1	**61**	1	1	0	0	0	0
30	0	1	0	0	0	1	**62**	0	1	0	0	0	0
31	1	0	0	0	0	1	**63**	1	0	0	0	0	0
32	0	0	0	0	1	1	**64**	0	0	0	0	0	0

Table B.1: Table of parameters

Ringraziamenti

Ritengo questo progetto di tesi, e in generale il percorso di questi cinque anni di università, un risultato non solo mio, ma di tutte le persone che con me hanno condiviso anche solo una piccola parte del cammino. Le poche righe che seguono vogliono essere un segno tangibile della vostra presenza e dell'apporto concreto che avete dato alla realizzazione di questa tappa del mio viaggio.

Ringrazio il prof. Alberto Berizzi e il Dott. Pietro Raboni (e con lui tutto il team di Engie-EPS) per la loro disponibilità e per il tempo che mi hanno dedicato durante l'elaborazione di questa tesi. Mi avete dato l'opportunità e i mezzi per sviluppare un progetto che mi ha appassionato e che sono fiero di aver svolto.

Ringrazio tutti i ragazzi del corso di Ingegneria Elettrica, in particolare i miei compagni di avventura in EPS: Francesco, Sergio, Alessandro e Massimo. Abbiamo trascorso insieme otto mesi intensi, pieni di alti e bassi. Nessuno meglio di voi conosce le difficoltà che ho incontrato, e siete stati lo sguardo amico e il supporto costante che mi ha aiutato a superarle.

Un ringraziamento particolare va alla mia famiglia, che in questi anni mi ha sempre incoraggiato, con pazienza, ad andare avanti, supportando tutte le mie scelte. Senza di voi e senza quello che mi avete insegnato, oggi non sarei qui.

Ringrazio i miei amici di sempre: Paolo, Michele e Stefano. Il confronto con voi sul piano umano è prezioso, e mi spinge a migliorarmi ogni giorno.

Ringrazio Monica, che tante volte mi ha raccolto e rimesso in piedi con amore. La tua forza è sempre un grande esempio per me, il compimento di questo percorso è in gran parte merito tuo.

Infine, un ringraziamento speciale va al nonno Elio. Tanti anni fa è stato il primo a spiegarmi che cos'è un ingegnere e a far nascere in me il sogno di diventarlo. Oggi voglio ricordarlo, nel giorno in cui quel sogno si realizza.